

---

# HOPSE: Scalable Higher-Order Positional and Structural Encoder for Combinatorial Representations

---

**Martin Carrasco** \*

University of Fribourg

[martin.carrasco@utec.edu.pe](mailto:martin.carrasco@utec.edu.pe)

**Guillermo Bernardez**

University California Santa Barbara

[guillermo\\_bernardez@ucsb.edu](mailto:guillermo_bernardez@ucsb.edu)

**Marco Montagna**

Sapienza University of Rome

[marco.montagna@uniroma1.it](mailto:marco.montagna@uniroma1.it)

**Nina Miolane**

University California Santa Barbara

[ninamiolane@ucsb.edu](mailto:ninamiolane@ucsb.edu)

**Lev Telyatnikov** \* †

Sapienza University of Rome

[lev.telyatnikov@uniroma1.it](mailto:lev.telyatnikov@uniroma1.it)

## Abstract

While Graph Neural Networks (GNNs) have proven highly effective at modeling relational data, pairwise connections cannot fully capture multi-way relationships naturally present in complex real-world systems. In response to this, Topological Deep Learning (TDL) leverages more general combinatorial representations –such as simplicial or cellular complexes– to accommodate higher-order interactions. Existing TDL methods often extend GNNs through Higher-Order Message Passing (HOMP), but face critical *scalability challenges* due to (i) a combinatorial explosion of message-passing routes, and (ii) significant complexity overhead from the propagation mechanism. To overcome these limitations, we propose HOPSE (Higher-Order Positional and Structural Encoder)–a *message passing-free* framework that uses Hasse graph decompositions to derive efficient and expressive encodings over *arbitrary higher-order domains*. Notably, HOPSE scales linearly with dataset size while preserving expressive power and permutation equivariance. Experiments on molecular, expressivity and topological benchmarks show that HOPSE matches or surpasses state-of-the-art performance while achieving up to 7× speedups over HOMP-based models, opening a new path for scalable TDL.

## 1 Introduction

Graph neural networks (GNNs) [46, 11] have demonstrated impressive capabilities in modeling relational data structured as graphs. However, their reliance on edges to encode interactions inherently limits them to pairwise relationships, which may not fully capture the complexity of many real-world systems. For instance, social dynamics often involve group interactions, while physical phenomena like electrostatic interactions in proteins can span multiple atoms simultaneously.

To address such limitations, Topological Deep Learning (TDL) [8, 23] introduces a framework for modeling multi-way interactions using *higher-order topological domains* such as hypergraphs, simplicial, cell, and combinatorial complexes. Within TDL, standard Topological Neural Networks

\* Authors for correspondence: [martin.carrasco@utec.edu.pe](mailto:martin.carrasco@utec.edu.pe), [lev.telyatnikovv@gmail.com](mailto:lev.telyatnikovv@gmail.com)

† The work was initiated while the author was pursuing their PhD at Sapienza University of Rome.

(TNNs) [18, 12, 22, 21, 38] extend the graph-based message passing paradigm through Higher-Order Message Passing (HOMP), enabling information flow across all of the dimensions of the considered combinatorial representation.<sup>3</sup> This generalization has shown strong performance across diverse fields—including social networks [30], protein biology [28], physics-informed learning [45], and computer networks [6, 5]—where interactions naturally extend beyond pairwise connections.

However, despite their theoretical advantages, TNNs face substantial challenges stemming from the HOMP paradigm. Unlike GNNs, TNNs’ ability to propagate information through the full hierarchy of a higher-order domain—where elements of different *ranks* (e.g., nodes, edges, faces, etc.) are interconnected—leads to an explosion in the number of possible sequences of *message passing routes* across these different levels [42, 33, 37]. More specifically, for a combinatorial complex  $\mathcal{T}$  with dimension—i.e. maximum rank— $R$ , a total of  $(R + 1)!$  message passing routes arises just considering communication flows between different ranks, and that number skyrockets to  $(R + 1)! \cdot (R + 1)^R$  when allowing same-rank connections (please see Appendix B for a detailed analysis).

On top of this vast architectural search space, TNNs operating under the HOMP paradigm are also known to be computationally demanding, message propagation often requiring significant processing resources even for moderately sized inputs [37, 20]. This combination of combinatorial design complexity and high computational cost *severely limits existing TNNs’ scalability*, posing a major barrier to their deployment in large-scale or time-sensitive real-world applications.

In response to these challenges, this work introduces ***Higher-Order Positional and Structural Encoder (HOPSE)***, a novel framework designed to overcome the computational hurdles associated with HOMP. Specifically, HOPSE main features and contributions include:

- **Higher-order topological encodings:** By exploiting Hasse graph decompositions—i.e. transformations of combinatorial representations into simpler graph ensembles [23, 38]—, HOPSE facilitates the efficient use of established graph positional and structural encoding techniques (e.g. [13]) to obtain analog representations for higher-order topological domains.
- **General message passing-free method:** Inspired by SaNN model [20], the proposed encoding-based methodology effectively captures relational information without explicit message passing mechanisms. Moreover, HOPSE is no longer constrained to simplicial complexes; by design, it can be applied to *any higher-order combinatorial representations*.
- **Scalability and computational efficiency:** In contrast to HOMP-based networks, HOPSE complexity scales linearly with respect to the number of elements in the combinatorial representation (Section 4.3). This is achieved by computing the encodings as a preprocessing step, significantly accelerating both training and inference (see Section 5 for experimental details).
- **Theoretical guarantees:** Even without message passing, HOPSE is as expressive as existing state-of-the-art HOMP-based models (e.g. Papillon et al. [38]) in distinguishing non-isomorphic complexes (Theorem 4.1), while preserving cell permutation equivariance (Theorem 4.2).
- **Flexible instantiations:** Two HOPSE realizations are presented—**HOPSE-M**, relying on hand-crafted graph-theoretical encodings, and **HOPSE-G**, using a pretrained GPSE encoder—offering complementary trade-offs between preprocessing cost and representational richness (Section 4.3).
- **Extensive empirical validation:** Comprehensive experiments on molecular benchmarks [34], CLS expressivity dataset [36], and MANTRA [2]—recent dataset consisting of pure topological tasks—validate the practical effectiveness of HOPSE, showcasing its ability to efficiently capture complex relational structures and outperform existing baselines—while being up to  $7\times$  faster than HOMP-based models (Section 5).

Additionally, Appendix B provides, for the first time, a detailed mathematical analysis of the combinatorial explosion of message passing routes in higher-order topological domains.

## 2 Background

This section introduces key concepts underpinning TDL. For brevity and generality, the following discussion centers on combinatorial complexes, which subsume all of the discrete topological domains

---

<sup>3</sup>The terms *higher-order topological domain* and *combinatorial representation* are used interchangeably: please see Appendix A.1 for the formal definitions.

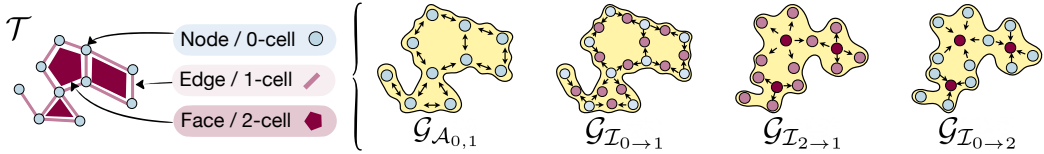


Figure 1: **Neighborhood expansions of a complex.** Given a complex  $\mathcal{T}$  (left), three examples of strictly augmented Hasse graphs  $\mathcal{G}_N$  are illustrated corresponding to 4 neighborhoods: adjacency of nodes w.r.t. edges ( $\mathcal{A}_{0,1}$ ), incidence from nodes to edges ( $\mathcal{I}_{0\rightarrow 1}$ ), incidence from faces to nodes ( $\mathcal{I}_{2\rightarrow 1}$ ), and incidence from nodes to faces ( $\mathcal{I}_{0\rightarrow 2}$ ).

leveraged by TDL [23]. Appendix A provides rigorous mathematical definitions of these other domains, such as simplicial and cellular complexes, along with an extended theoretical background.

**Combinatorial complex.** A *combinatorial complex*  $\mathcal{T}$  is a triple  $(\mathcal{V}, \mathcal{C}, \text{rk})$  consisting of a set  $\mathcal{V}$ , a subset  $\mathcal{C}$  of the powerset  $\mathcal{P}(\mathcal{V}) \setminus \emptyset$ , and a rank function  $\text{rk} : \mathcal{C} \rightarrow \mathbb{Z}_{\geq 0}$  with the following properties:

1. For all  $v \in \mathcal{V}$ ,  $\{v\} \in \mathcal{C}$  and  $\text{rk}(\{v\}) = 0$ ;
2. The function  $\text{rk}$  is order-preserving, i.e., if  $\sigma, \tau \in \mathcal{C}$  satisfy  $\sigma \subseteq \tau$ , then  $\text{rk}(\sigma) \leq \text{rk}(\tau)$ ;

The elements of  $\mathcal{V}$  represent the nodes, while the elements of  $\mathcal{C}$  are called cells (i.e., groups of nodes). The cell  $\sigma \in \mathcal{C}$  of rank  $k := \text{rk}(\sigma)$  is referred to as a  $k$ -cell.  $\mathcal{C}$  simplifies notation for  $(\mathcal{V}, \mathcal{C}, \text{rk})$ . Lastly, the dimension of  $\mathcal{T}$  is defined as the maximal rank among its cells:  $\dim(\mathcal{T}) := \max_{\sigma \in \mathcal{C}} \text{rk}(\sigma)$ .

**Signals over combinatorial complexes.** A combinatorial complex  $\mathcal{T} = (\mathcal{V}, \mathcal{C}, \text{rk})$  can be equipped with signals, generalizing the concept of featured graph<sup>4</sup> (see Definition A.1) to higher-order structures. In this context, a signal is a set of functions  $\mathcal{F} = \{F_r\}_{r \geq 0}$ , where  $F_r : \{\sigma \in \mathcal{C} \mid \text{rk}(\sigma) = r\} \rightarrow \mathbb{R}^{D_r}$ , where  $D_r$  is the dimension of the feature space for rank- $r$  cells. For this work, it is important to emphasize that a complex can have multiple attribute functions over each  $r$ -cell. More formally,  $\mathcal{F} = \{F_{r,k}\}_{k=1}^K$  for all  $r \geq 0$ , where each  $F_{r,k}$  shares the same domain:  $\text{Dom}(F_{r,k}) = \text{Dom}(F_r)$ .

**Neighborhood relations: adjacencies and incidences.** Combinatorial complexes can be equipped with a notion of neighborhood among cells that induces rich topological structures. Formally, denoting by  $\mathcal{P}(\cdot)$  the power set, a neighborhood function  $\mathcal{N} : \mathcal{C} \rightarrow \mathcal{P}(\mathcal{C})$  on a complex  $\mathcal{T}$  maps each cell  $\sigma \in \mathcal{C}$  to a collection of *neighbor cells*  $\mathcal{N}(\sigma) \subset \mathcal{C} \cup \emptyset$ . Traditional neighborhood functions include *adjacencies* ( $\mathcal{A}_{t,s}$ ), connecting cells of the same rank  $t$  –through adjacency relations w.r.t. cells of another rank  $s$ –, and *incidences* ( $\mathcal{I}_{s\rightarrow t}$ ), linking cells of different ranks –from a source rank  $s$  to a target rank  $t$ . Figure 1 presents some instances, and Appendix A.2 provides formal definitions.

**Strictly augmented Hasse graphs.** Given a complex  $\mathcal{T}$ , each particular neighborhood  $\mathcal{N}$  induces a strictly augmented Hasse graph  $\mathcal{G}_N = (\mathcal{C}_N, \mathcal{E}_N)$  [39], defined as the directed graph whose nodes and edges are given, respectively, by

$$\mathcal{C}_N = \{\sigma \in \mathcal{C} \mid \mathcal{N}(\sigma) \neq \emptyset\} \quad \text{and} \quad \mathcal{E}_N = \{(\tau, \sigma) \mid \sigma, \tau \in \mathcal{C}_N, \tau \in \mathcal{N}(\sigma)\}.$$

Figure 1 visually shows some examples of these neighborhood graph expansions. Notably, “strictly” comes from the fact that the set of nodes of  $\mathcal{G}_N$  is restricted to  $\mathcal{C}_N$ , i.e., to those cells that have at least one neighbor according to  $\mathcal{N}$ . In contrast to this, the original definition of *augmented Hasse graph* considers the full set of cells  $\mathcal{C}$  [23].

### 3 Related works

**Positional and Structural Encodings in GNNs.** In the graph domain, a range of positional and structural encodings (PSEs) have been proposed to enhance node representations. Positional encodings typically capture a node’s location within the graph (e.g., via distances or coordinates), while structural encodings describe the node’s role or function in the topology (e.g., node degrees). Classical approaches of positional encodings include spectral methods based on Laplacian eigenvectors (LapPE) [17], while a common structural encoding is the random-walk embedding (RWSE) [15, 43], which reflects multi-hop connectivity; these handcrafted features help differentiate nodes with otherwise similar local neighborhoods. More recently, transformer-based GNNs have incorporated PSEs

<sup>4</sup>Attributed graph and featured graph are used interchangeably to comply with the literature.

into attention mechanisms [14, 40, 31]. Other works focus on decoupling the positional information from the structure and learn the embeddings instead of picking them manually [14]. Building upon this, the Graph Positional and Structural Encoder (GPSE) [13] offers a unified and transferable solution by learning a shared latent space of PSEs through self-supervised pretraining. GPSE’s embeddings can be integrated into downstream GNNs, achieving performance on par with or exceeding task-specific encodings, and advancing the development of general-purpose graph models.

**Combinatorial Complex Neural Networks.** To overcome the pairwise limitations of graphs, recent work has turned to explicit representation of higher-order interactions through topological domains. Combinatorial complexes provide a unified framework for modeling higher-order interactions with hierarchical organization, and their associated Combinatorial Complex Neural Networks (CCNNs) enable message passing across cells of varying rank (HOMP paradigm), naturally capturing multi-way relationships [23]. Generalizing and subsuming CCNNs, Generalized CCNNs (GCCNs) [39] offer a more flexible and powerful framework: they systematically decompose a complex into a set of strictly augmented Hasse graphs –each one capturing a particular neighborhood– in a modular way that preserves the higher-order structure. In doing so, GCCNs not only facilitate the design of new TNN architectures but also help bridge the gap between graph deep learning and TDL. However, existing TNNs –CCNNs and GCCNs alike– suffer from the high computational complexity associated to HOMP, limiting their practical use in large real-world applications.

**Positional encodings in higher-order domains.** Encoding positional information for higher-order topological elements poses unique challenges. Unlike in graphs, where positional features are typically assigned to nodes, each cell rank of a combinatorial complex –nodes, edges, faces,...– potentially requires its own descriptor. Recent works have begun addressing this, though this topic still remains largely unexplored. For instance, the Cellular Transformer (CT) [1] extends transformer architectures to cell complexes by incorporating attention mechanisms that respect higher-order incidence relations. To support this, the authors introduce a set of manually crafted positional encodings tailored to cellular complexes, though their results did not shed light on how to build robust encodings—different ones perform best on different tasks. Moreover, CT incurs quadratic complexity in the number of cells due to the attention mechanism, limiting its scalability to medium-to-large scenarios. In contrast, Simplicial-aware Neural Networks (SANN) [20] take a more efficient route by bypassing message passing entirely. SANN precomputes structural and positional summaries (e.g., over lower, upper, and co-neighbors) and feeds them as fixed-length vectors into a standard neural network. This achieves constant runtime and memory overhead while maintaining strong expressivity and performance. Nevertheless, the SANN architecture is also constrained in terms of the topological domain (simplicial complex-specific), as well as with the choices of neighborhoods –which haves an impact into its theoretical expressivity and applicability.

## 4 HOPSE: higher-order positional and structural encoder

Section 4.1 outlines the proposed HOPSE pipeline, Section 4.2 establishes its theoretical guarantees, and Section 4.3 presents two practical realizations of the framework.

Let  $\mathcal{T}$  be an arbitrary combinatorial complex, and  $\mathcal{N}_C \subset \mathcal{N}_{\mathcal{T}}$  any subset of neighborhoods on  $\mathcal{T}$ . The following **notation** is introduced to support the upcoming presentation of the framework:

**Strictly augmented multi-attributed Hasse graphs.** For a given neighborhood  $\mathcal{N} \in \mathcal{N}_C$ , its *strictly augmented multi-attributed Hasse graph* –denoted by  $\mathcal{J}_{\mathcal{N}}$ – assigns to the resulting strictly augmented Hasse graph  $\mathcal{G}_{\mathcal{N}}$  the corresponding signals  $\mathcal{F}_{\mathcal{N}}$  over the cells present in that neighborhood, i.e.  $\mathcal{J}_{\mathcal{N}} = (\mathcal{C}_{\mathcal{N}}, \mathcal{E}_{\mathcal{N}}, \mathcal{F}_{\mathcal{N}})$ . The shorthand  $\mathcal{F}_{\mathcal{N},k} = \{F_{r,k}\}_{r \geq 0}$  is the set of all  $k$ -attribute functions for each rank  $r$  that act on the subset of cells in a neighborhood  $\mathcal{C}_{\mathcal{N}}$  as  $F_{r,k} : \{\sigma \in \mathcal{C}_{\mathcal{N}}\} \rightarrow \mathbb{R}^{D_r}$ . To streamline the management of multiple associated signals, the *restriction* of  $\mathcal{J}_{\mathcal{N}}$  to the  $k$ -th feature is defined as  $\mathcal{J}_{\mathcal{N}}|_k = (\mathcal{C}_{\mathcal{N}}, \mathcal{E}_{\mathcal{N}}, \mathcal{F}_{\mathcal{N},k})$ . Lastly,  $\mathbf{J}_C = \{\mathcal{J}_{\mathcal{N}}\}_{\mathcal{N} \in \mathcal{N}_C}$  denotes the corresponding *Hasse graph decomposition* of  $\mathcal{T}$  w.r.t. a given neighborhood set  $\mathcal{N}_C$ .

**Rank-targeted neighborhoods.** The *rank-targeted neighborhood* is defined as the collection of neighborhood functions whose target cells have the same fixed rank  $r$ :  $\mathcal{N}^{\rightarrow r} := \{\mathcal{N} \in \mathcal{N}_C \mid \forall \sigma \in \mathcal{C}, \forall \tau \in \mathcal{N}(\sigma) : \text{rk}(\tau) = r\}$ .

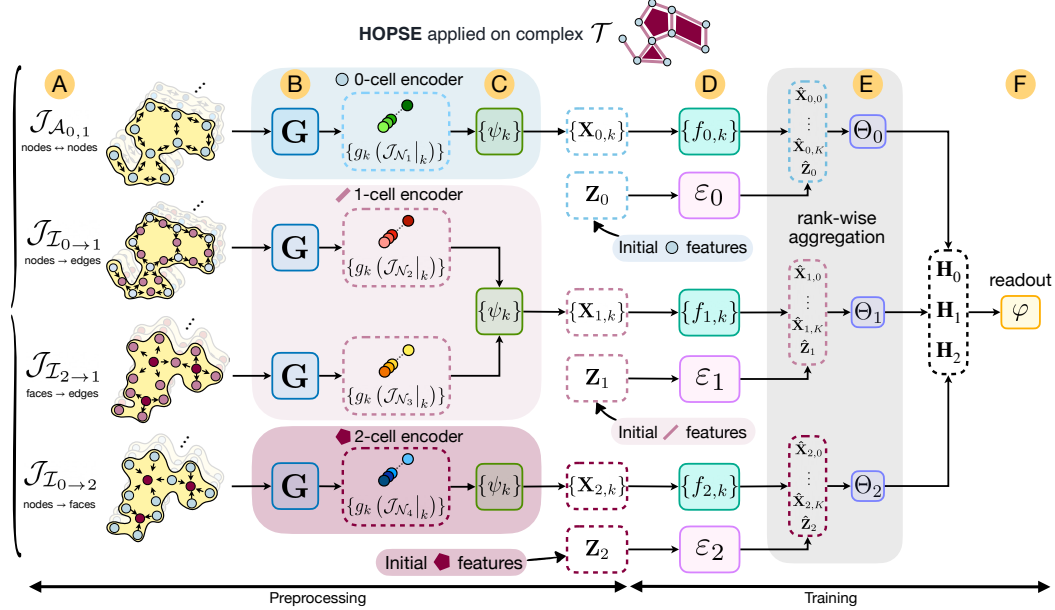


Figure 2: **HOPSE pipeline.** (A) Considering the collection of neighborhoods  $\mathcal{N}_C = \{\mathcal{A}_{0,1}, \mathcal{I}_{0 \rightarrow 1}, \mathcal{I}_{2 \rightarrow 1}, \mathcal{I}_{0 \rightarrow 2}\}$ , the input combinatorial complex  $\mathcal{T}$  is decomposed into the corresponding multi-attributed Hasse graphs expansions  $\{\mathcal{J}_N\}_{\mathcal{N}_C}$ —each one with  $k$  associated signals. (B) Positional and structural encodings are computed for each Hasse graph,  $\mathbf{G}(\mathcal{J}_N)$ , as defined in Equation (1). (C) Higher-order PS encodings are derived via the target rank-aware aggregation  $\psi_k$  (see Equation (2)). (D) The PS encodings  $\mathbf{X}_{r,k}$  are transformed using  $f_{r,k}(\cdot)$ , and initial cell features  $\mathbf{Z}_r$  are embedded via  $\varepsilon_r(\cdot)$ , following Equations (3) and (4). (E) Rank-specific, neighborhood-aware representations  $\mathbf{H}_r$  are learned using  $\Theta_r(\cdot)$ , as described in Equation (5). (F) The final task-specific readout  $\varphi(\cdot)$  integrates all  $\mathbf{H}_r$  representations (Equation (6)).

#### 4.1 Methodology

This section describes HOPSE, a method for enriching cell features in combinatorial complexes with higher-order positional and structural encodings derived from Hasse graph decompositions. HOPSE enables expressive higher-order modeling without relying on the computational overhead of HOMP, while retaining its representational power. The full pipeline is illustrated in Figure 2, with components referenced using the corresponding labels (A–F) throughout this section.

**Extract positional and structural information.** Let  $\mathcal{N}_C$  be a collection of neighborhood functions. For each neighborhood  $\mathcal{N} \in \mathcal{N}_C$ , the Hasse graph decomposition of  $\mathcal{T}$  enables the treatment of every  $\mathcal{J}_N$  as an independent component (see Figure 2A), each representing a unique set of connectivity relationships.  $\mathbf{G}$  is a set of Positional and Structural Encoders (PSEs) such that

$$\mathbf{G}: \{1, \dots, K\} \times \mathcal{J}_C \longrightarrow \mathbb{R}^{N \times D_k}, \quad (k, \mathcal{J}_N) \mapsto g_k(\mathcal{J}_N|_k). \quad (1)$$

Here  $g_k(\cdot) : \mathcal{J}_C \rightarrow \mathbb{R}^{|\mathcal{C}_N|_{\text{target}} \times D_k}$  denotes a particular PSE, with  $|\mathcal{C}_N|_{\text{target}}$  being the number of nodes in the Hasse graph induced by neighborhood  $\mathcal{N}$  corresponding to the target cells (illustrated in Figure 2B). Note that each  $g_k(\cdot)$  maps to a different  $D_k$ , allowing PSEs to have different dimensions.

**Aggregate positional and structural encodings across neighborhoods.** The proposed neighborhood aggregation mechanism  $\psi_k(\cdot)$  operates by grouping the encodings of cells with the same target rank  $r$  to produce a unique embedding for each cell and each  $k \in \{1, \dots, K\}$  (see Figure 2C). The embeddings for cells of rank  $r$  are computed as:

$$\mathbf{X}_{r,k} = \psi_k(\{g_k(\mathcal{J}_N|_k) \mid \mathcal{N} \in \mathcal{N}^{\rightarrow r}\}), \quad (2)$$

where  $\mathbf{X}_{r,k} \in \mathbb{R}^{N_r \times D_{k'}}$ , with  $N_r$  denoting the number of  $r$ -cells and  $D_{k'}$  representing the output feature dimension for attribute  $k$ . The functions  $\psi_k(\cdot)$  can also be interpreted as rank-level aggregators, where the aggregation operation can be any standard reduction method. Common choices include concatenation, sum, average, or even learnable transformations such as MLPs. The main advantage of using non-learnable aggregation functions for  $\psi_k$  is that the embeddings  $\mathbf{X}_{r,k}$  can be precomputed during dataset preprocessing, since they do not require learning.

**Learning embeddings of cells.** In the HOPSE framework, each  $r$ -cell is associated with two complementary sources of information: (i) higher-order positional and structural encodings  $\mathbf{X}_{r,k}$  aggregated from multiple neighborhoods, and (ii) initial features  $\mathbf{Z}_r$  provided by the dataset or derived during the construction of the higher-order structure. Both types of features are independently projected into latent spaces through sets of learnable functions (see Figure 2D):

$$\hat{\mathbf{X}}_{r,k} = f_{r,k}(\mathbf{X}_{r,k}), \quad (3)$$

$$\hat{\mathbf{Z}}_r = \varepsilon_r(\mathbf{Z}_r), \quad (4)$$

where  $f_{r,k}(\cdot)$  is applied to each feature  $k$  of the  $r$ -cells, and  $\varepsilon_r(\cdot)$  to their initial features.

**Learning neighborhood-aware representations.** Next, to integrate the structural information with the cells’ initial attributes, the extracted and transformed higher-order PS encodings and the cell features are passed through the aggregator  $\Theta_r(\cdot)$  (see Figure 2E) to obtain the final neighborhood-aware representations  $\mathbf{H}_r \in \mathbb{R}^{N_r \times D_r}$ :

$$\mathbf{H}_r = \Theta_r(\hat{\mathbf{Z}}_r, \hat{\mathbf{X}}_{r,1}, \dots, \hat{\mathbf{X}}_{r,K}), \quad (5)$$

**Learning the downstream task.** Since the structural information is now contained in the cell features, they can be treated independently. For example, for *complex-level* tasks where the network needs an output for the whole complex, the global transformation  $\varphi(\cdot)$  combines the aggregated embeddings from all ranks (see Figure 2F). The overall output is

$$\text{HOPSE}(\mathcal{T}) = \varphi(\mathbf{H}_0, \mathbf{H}_1, \dots, \mathbf{H}_R). \quad (6)$$

## 4.2 Theoretical guarantees

The expressivity of GNNs is commonly analyzed through their correspondence with the Weisfeiler–Leman (WL) isomorphism test [26]. In the context of TDL, a generalization of WL over arbitrary neighborhoods of a combinatorial complex (CC) has been proposed, referred to as the CCWL test [39]. The following theorem establishes the expressivity of HOPSE with respect to it.

**Theorem 4.1.** *HOPSE is more powerful than the CCWL test in distinguishing non-isomorphic combinatorial complexes if the functions  $\varepsilon_r(\cdot)$ ,  $g_k(\cdot)$ ,  $\psi_k(\cdot)$ ,  $f_{r,k}(\cdot)$ , and  $\Theta_r(\cdot)$  are injective for all  $k \in 1, \dots, K$  and for all  $r \in 0, \dots, R$ .*

The proof idea is that although HOPSE does not rely on message passing, with appropriately chosen neighborhoods, it can compute positional encodings using the same information as CCWL. Given the injectivity assumptions, this implies at least equal expressivity. The proof concludes by showing two CCs distinguished by HOPSE but not by CCWL. Full details are in Appendix C.

Another key property for models working on combinatorial data is cell permutation equivariance—the ability to yield consistent outputs under permutations of the cells. The following theorem establishes that HOPSE preserves this property under reasonable conditions:

**Theorem 4.2.** *HOPSE is cell permutation equivariant if the functions  $\varepsilon_r(\cdot)$ ,  $g_k(\cdot)$ ,  $\psi_k(\cdot)$ ,  $f_{r,k}(\cdot)$ , and  $\Theta_r(\cdot)$  are cell permutation equivariant for all  $k \in 1, \dots, K$  and all  $r \in 0, \dots, R$ .*

This follows from the fact that compositions of permutation-equivariant functions remain equivariant. The proof is in Appendix C. While this requirement may seem strong, standard MLPs—though not equivariant to feature permutations—are equivariant to permutations of input sets, making them suitable functions for  $\varepsilon_r(\cdot)$ ,  $f_{r,k}(\cdot)$ , and  $\Theta_r(\cdot)$ .

## 4.3 Realization of the framework

The practical implementation of the proposed framework requires defining a set of neighborhoods of interest  $\mathcal{N}_C = \{\mathcal{N}_1, \dots, \mathcal{N}_T\}$  (discussed in Section 5), a set of encoding functions  $\mathbf{G}$  for deriving structural and positional features, neighborhood aggregation functions  $\psi_k(\cdot)$ , rank-specific processing functions  $f_{r,k}(\cdot)$ , and a structure mixing function  $\Theta_r(\cdot)$ . In particular, this work adopts  $\psi_k(\cdot) = \text{CONCAT}(\cdot)$  for aggregation, enabling each positional encoding to be handled independently. For both  $f_{r,k}(\cdot)$  and  $\Theta_r(\cdot)$ , trainable multilayer perceptrons (MLPs) are used. The choice of encoding

functions  $\mathbf{G}$  defines the two proposed instantiations of the framework, **HOPSE-M** and **HOPSE-G**, offering a trade-off regarding the informativeness of extracted PS encoding and the computation cost to generate them. Additional implementation details are provided in Appendix D.

**HOPSE-M.** This realization incorporates manually selected positional and structural encodings commonly used in graph learning. Specifically,  $\mathbf{G} = \{g_1, g_2, g_3, g_4\}$  includes: (i) eigenvector-based encodings, (ii) electrostatic potential-based encodings, (iii) random-walk-based encodings, and (iv) heat kernel signatures. These encodings are chosen to provide a fair comparison with HOPSE-G, as the GPSE model used in that variant was trained on the same set of positional and structural descriptors [13]. While informative, several of these encodings—especially those requiring eigendecomposition such as (i), (ii), and (iv)—are computationally intensive, with complexity  $\mathcal{O}(n^3)$  with  $n$  the number of graph nodes.

**HOPSE-G.** This variant leverages the pretrained GPSE network [13] to encode structural and positional information through a lightweight message-passing architecture. In this realization,  $\mathbf{G} = \{g_1\}$  with  $g_1 = \text{GPSE}(\cdot)$ . Unlike manual encodings that rely on computationally intensive operations such as eigendecomposition, GPSE produces latent descriptors using standard message passing. This makes **HOPSE-G** particularly suitable for large combinatorial complexes with many cells, offering a scalable alternative without significant loss in expressiveness.

**Computational complexity.** The presented implementation of HOPSE is designed for computational efficiency: no training is required up to and including Equation (2), allowing the matrices  $\mathbf{X}_{r,k}$  to be fully precomputed in a preprocessing phase. By offloading all structure-dependent computations to preprocessing, HOPSE has complexity that scales linearly with the number of cells while retaining high expressive power, as established in Theorem 4.1. The efficiency of this design is further validated by experimental runtime results in Table 3. A comprehensive complexity analysis and a comparison with GCCN—a highly general higher-order architecture—are provided in Appendix E.

## 5 Experiments

This section empirically evaluates the proposed HOPSE framework, benchmarked against state-of-the-art TNNs. Both instantiations of the framework, **HOPSE-M** and **HOPSE-G** (see Section 4.3), are assessed on graph molecular datasets, as well as on expressivity and topological tasks. The standardized experimental protocol introduced in TopoBench [42] is adopted to ensure fair and reproducible comparisons through a comprehensive optimization and evaluation suite. The experimental setup is carefully designed to systematically address the following research questions:

- Q1.** Can the proposed HOPSE framework and its realizations (**HOPSE-M** and **HOPSE-G**) effectively approximate the performance of TNNs that leverage HOMP on standard TDL datasets?
- Q2.** Can HOPSE achieve competitive performance on synthetic datasets specifically constructed to evaluate the ability to capture and utilize topological properties?
- Q3.** How expressive HOPSE can get in practical scenarios compared with other GNNs and TNNs?
- Q4.** To what extent does the reduced complexity of HOPSE, relative to HOMP-based methods, yield practical improvements in execution cost and scalability on standard TDL benchmarks?

### 5.1 Evaluation setup

**Datasets.** First, the framework is evaluated on five standard benchmarking datasets commonly used in the TDL literature [42], comprising four graph classification tasks and one graph regression task. The classification tasks use datasets from the TUDataset collection<sup>5</sup>—MUTAG, PROTEINS, NCI1, and NCI109 [35]. For regression, the ZINC dataset is used [27]. Following standard practice in TDL, structural lifting is applied to lift these graph datasets into higher-order domains—specifically, cycle-based lifting for the cell domain and clique complex lifting for the simplicial domain. Next, MANTRA family [2] represents purely topological datasets and tasks. It comprises over 43,000 triangulations of 2-manifolds. Among the multiple classification tasks that MANTRA datasets offer, this analysis

<sup>5</sup>Although these datasets are relatively dated, they remain widely adopted as a benchmarking suite in TDL research, offering consistent baselines for comparative evaluation

Table 1: Accuracy on benchmark datasets. Results are shown as mean  $\pm$  standard deviation. The best results are highlighted in **bold**, and those within one standard deviation of the best are in blue.

Model	Graph Tasks					Topological Tasks			
	MUTAG ( $\uparrow$ )	PROTEINS ( $\uparrow$ )	NCI1 ( $\uparrow$ )	NCI109 ( $\uparrow$ )	ZINC ( $\downarrow$ )	NAME ( $\uparrow$ )	ORIENT ( $\uparrow$ )	$\beta_1$ ( $\uparrow$ )	$\beta_2$ ( $\uparrow$ )
Graph	GCN	69.79 $\pm$ 6.80	75.70 $\pm$ 2.14	72.86 $\pm$ 0.69	72.20 $\pm$ 1.22	0.62 $\pm$ 0.01	42.14 $\pm$ 2.72	47.94 $\pm$ 0.00	46.86 $\pm$ 4.50
	GAT	72.77 $\pm$ 2.77	76.34 $\pm$ 1.66	75.00 $\pm$ 0.99	73.80 $\pm$ 0.73	0.61 $\pm$ 0.01	18.09 $\pm$ 0.65	47.94 $\pm$ 0.00	7.45 $\pm$ 0.05
	GIN	79.57 $\pm$ 6.13	75.20 $\pm$ 3.30	74.26 $\pm$ 0.96	74.42 $\pm$ 0.70	0.57 $\pm$ 0.04	76.14 $\pm$ 0.14	56.28 $\pm$ 0.45	88.13 $\pm$ 0.00
	SCN	73.62 $\pm$ 6.13	75.27 $\pm$ 2.14	74.49 $\pm$ 1.03	75.70 $\pm$ 1.04	0.53 $\pm$ 0.04	79.48 $\pm$ 1.36	69.55 $\pm$ 0.97	76.45 $\pm$ 3.06
	SCCNN	76.17 $\pm$ 6.63	74.19 $\pm$ 2.86	76.60 $\pm$ 1.75	77.12 $\pm$ 1.07	0.36 $\pm$ 0.02	<b>95.08 <math>\pm</math> 0.56</b>	<b>86.29 <math>\pm</math> 1.23</b>	90.20 $\pm$ 0.20
	SaNN	79.57 $\pm$ 3.56	75.05 $\pm$ 3.52	68.75 $\pm$ 1.64	68.17 $\pm$ 0.88	0.55 $\pm$ 0.01	81.76 $\pm$ 1.37	61.65 $\pm$ 0.55	88.46 $\pm$ 0.09
Simplicial	GCCN	85.96 $\pm$ 4.66	74.91 $\pm$ 2.51	76.85 $\pm$ 1.50	75.76 $\pm$ 1.28	0.35 $\pm$ 0.01	86.76 $\pm$ 1.27	76.60 $\pm$ 1.67	84.20 $\pm$ 4.80
	HOPSE-M	86.38 $\pm$ 6.31	75.13 $\pm$ 3.66	77.35 $\pm$ 0.81	76.34 $\pm$ 1.40	0.39 $\pm$ 0.02	91.50 $\pm$ 1.45	80.68 $\pm$ 1.72	<b>90.26 <math>\pm</math> 0.55</b>
	HOPSE-G	85.53 $\pm$ 2.77	76.27 $\pm$ 2.10	77.70 $\pm$ 1.40	76.36 $\pm$ 1.75	0.43 $\pm$ 0.01	81.75 $\pm$ 1.26	62.17 $\pm$ 0.98	<b>71.69 <math>\pm</math> 1.50</b>
	CCCN	77.02 $\pm$ 9.32	73.33 $\pm$ 2.30	76.67 $\pm$ 1.48	75.35 $\pm$ 1.50	0.34 $\pm$ 0.02	-	-	-
	CWN	80.43 $\pm$ 1.78	76.13 $\pm$ 2.70	73.93 $\pm$ 1.87	73.80 $\pm$ 2.06	0.34 $\pm$ 0.01	-	-	-
	GCCN	86.38 $\pm$ 6.49	74.41 $\pm$ 1.77	78.23 $\pm$ 1.47	77.19 $\pm$ 0.21	<b>0.19 <math>\pm</math> 0.00</b>	-	-	-
Cell	HOPSE-M	<b>88.09 <math>\pm</math> 5.55</b>	<b>76.99 <math>\pm</math> 2.63</b>	78.09 $\pm$ 1.44	77.27 $\pm$ 1.01	0.25 $\pm$ 0.01	-	-	-
	HOPSE-G	<b>88.09 <math>\pm</math> 1.90</b>	76.42 $\pm$ 2.19	<b>79.07 <math>\pm</math> 0.65</b>	<b>77.81 <math>\pm</math> 1.26</b>	0.21 $\pm$ 0.01	-	-	-

focuses on the following three: predicting the homeomorphism name, predicting the orientability of a triangulated surface, and assigning a numerical label to the first three Betti numbers  $\beta_0$ ,  $\beta_1$ , and  $\beta_2$ . Lastly, the evaluation includes the CLS dataset [36], used to assess the expressivity of GNNs [16], which contains 150 graphs across 10 isomorphism classes. For further details, see Appendix F.

**Models.** The SANN architecture is re-implemented due to unavailable source code [19] and included in all benchmarks. For the MANTRA family [2], baseline results are reported for the first time under the TopoBench protocol, ensuring consistency with the broader evaluation framework. Full details of the hyperparameter search and selected configurations are provided in Appendix F.2.

**Training and evaluation.** To ensure fair comparisons, five stratified splits with a 50%/25%/25% train/validation/test ratio are considered for each dataset and task –except on ZINC, which uses predefined splits [27]. The optimal hyperparameter configuration is selected based on the average validation performance across five random seeds. Evaluation metrics include classification accuracy (MUTAG, PROTEINS, NCI1, NCI109), mean absolute error (MAE; ZINC), and F1 score (MANTRA). For each dataset, the mean and standard deviation are computed across the five test sets and reported in Table 1. Publicly available results are adopted from Telyatnikov et al. [42] and Papillon et al. [39] where applicable for graph datasets.

## 5.2 Experimental Results

**Accuracy comparison.** Table 1 presents a performance comparison across topological domains: graph, simplicial, and cell. The proposed **HOPSE-M** and **HOPSE-G** models demonstrate consistently strong performance, particularly in the simplicial domain, answering both **Q1.** and **Q2.** affirmatively. On standard graph classification benchmarks used in TDL, both HOPSE variants match or outperform most baselines, with **HOPSE-M** ranking among the top models and achieving state-of-the-art results in several cases (PROTEINS, NCI1, NCI109). While the performance gap on ZINC highlights the advantage of message-passing in fine-grained molecular regression tasks, HOPSE still remains competitive without relying on the HOMP procedure. The most significant gains are observed on the pure topological datasets. **HOPSE-M** delivers the strongest results on  $\beta_1$  and  $\beta_2$ , outperforming all baselines, including models with explicit simplicial message passing. This suggests that HOPSE can effectively encode and leverage topological structure. In summary, the HOPSE framework achieves strong performance across both graph and synthetic topological benchmarks, demonstrating that a carefully designed structural encoding pipeline can approximate or surpass topological message-passing methods. Detailed analysis of the results is provided in Appendix F.

**Empirical expressivity.** Table 2 reports the mean, minimum, and maximum test classification accuracy over five folds for the best-performing baselines, covering all domains. The results show that SANN and SCNN slightly outperform baseline MP-GNNs, while GCCN performs better on

Table 3: Runtime in seconds. Results are shown as mean  $\pm$  standard deviation. The fastest model per domain is in **bold** and those that are within one standard deviation of the best are in **blue**.

Model	Graph Tasks					Topological Tasks		
	MUTAG	PROTEINS	NCI1	NCI109	ZINC	NAME ( $\uparrow$ )	ORIENT	$(\beta_0, \beta_1, \beta_2)$
Graph	GCN	<b>4 <math>\pm</math> 1</b>	<b>8 <math>\pm</math> 2</b>	<b>53 <math>\pm</math> 20</b>	<b>37 <math>\pm</math> 9</b>	<b>147 <math>\pm</math> 28</b>	<b>3538 <math>\pm</math> 38</b>	<b>3534 <math>\pm</math> 49</b>
	GAT	<b>4 <math>\pm</math> 1</b>	<b>8 <math>\pm</math> 2</b>	<b>57 <math>\pm</math> 17</b>	56 $\pm$ 9	171 $\pm$ 65	3589 $\pm$ 84	3544 $\pm$ 44
	GIN	5 $\pm$ 1	9 $\pm$ 2	61 $\pm$ 24	50 $\pm$ 8	168 $\pm$ 107	3568 $\pm$ 44	3536 $\pm$ 46
Simplicial	SCN	8 $\pm$ 2	43 $\pm$ 13	276 $\pm$ 63	226 $\pm$ 66	1210 $\pm$ 572	5115 $\pm$ 653	4773 $\pm$ 193
	SCCNN	14 $\pm$ 3	54 $\pm$ 11	307 $\pm$ 83	354 $\pm$ 106	2060 $\pm$ 408	5521 $\pm$ 319	6920 $\pm$ 1524
	SaNN	9 $\pm$ 2	50 $\pm$ 12	250 $\pm$ 18	211 $\pm$ 66	1263 $\pm$ 252	5572 $\pm$ 1053	4619 $\pm$ 103
	GCCN	61 $\pm$ 7	66 $\pm$ 21	904 $\pm$ 180	538 $\pm$ 39	3603 $\pm$ 475	5898 $\pm$ 1961	4564 $\pm$ 631
	HOPSE-M	<b>7 <math>\pm</math> 2</b>	<b>38 <math>\pm</math> 8</b>	<b>164 <math>\pm</math> 79</b>	219 $\pm$ 26	1061 $\pm$ 405	<b>3596 <math>\pm</math> 519</b>	3409 $\pm$ 162
	HOPSE-G	<b>5 <math>\pm</math> 0</b>	<b>33 <math>\pm</math> 8</b>	<b>130 <math>\pm</math> 22</b>	<b>107 <math>\pm</math> 28</b>	<b>478 <math>\pm</math> 107</b>	3324 $\pm$ 1113	<b>2795 <math>\pm</math> 112</b>
Cell	CCCN	12 $\pm$ 2	42 $\pm$ 7	372 $\pm$ 109	272 $\pm$ 21	1621 $\pm$ 142	-	-
	CWN	11 $\pm$ 1	54 $\pm$ 18	302 $\pm$ 63	295 $\pm$ 46	1390 $\pm$ 97	-	-
	GCCN	61 $\pm$ 18	59 $\pm$ 18	523 $\pm$ 119	386 $\pm$ 76	3301 $\pm$ 440	-	-
	HOPSE-M	<b>7 <math>\pm</math> 1</b>	<b>37 <math>\pm</math> 7</b>	<b>147 <math>\pm</math> 24</b>	<b>122 <math>\pm</math> 18</b>	<b>1313 <math>\pm</math> 132</b>	-	-
	HOPSE-G	<b>7 <math>\pm</math> 1</b>	<b>32 <math>\pm</math> 5</b>	<b>153 <math>\pm</math> 8</b>	<b>104 <math>\pm</math> 38</b>	<b>1230 <math>\pm</math> 527</b>	-	-

the cell domain but still falls short of 3WLGNN. **HOPSE-M** perfectly distinguishes all isomorphism classes, and **HOPSE-G** achieves the second-best position (**Q3.**).

**Computation time comparison.** To highlight the efficiency of HOPSE, Table 3 reports the total runtime in seconds. Notably, either **HOPSE-G** or **HOPSE-M** achieves the fastest overall runtime across both simplicial and cell domains. On graph datasets, the speedup can reach up to 7x—for example, **HOPSE-G** runs in 130 seconds compared to 904 seconds for GCCN on NCI1, while also delivering better performance. On average, **HOPSE-M** and **HOPSE-G** outperform the most competitive baselines with speedups of 1.5x and 3x over SCCN, and 3x and 5x over GCCN, respectively, while achieving top results on 6 out of 9 datasets. Overall, both models significantly reduce runtime while delivering competitive or superior accuracy (**Q4.**).

**Choice of  $\mathcal{N}_C$ .** The neighborhood set  $\mathcal{N}_C$  is a critical design choice in the HOPSE framework, influencing both the expressivity and computational behavior of the model. Performed ablation studies (Appendix F) reveal that richer (i.e. larger and diverse) neighborhood configurations consistently yield top or near-top accuracy across complex datasets—e.g. MANTRA’s topological tasks, ZINC—as shown in Tables 6 and 7. Importantly, these gains come without significant runtime penalties: as demonstrated in Tables 10 and 11, per-epoch runtime remains almost stable, and total runtime often decreases due to faster convergence. Notably, the cell domain strongly aligns with expressivity and efficiency, especially on molecular tasks. These findings suggest a practical guideline: practitioners aiming for strong performance without exhaustive search over all neighborhood configurations can safely opt for larger  $\mathcal{N}_C$  sets. This choice is especially advantageous for complex tasks, balancing predictive power, convergence speed, and runtime efficiency (**Q1., Q2., Q4.**).

## 6 Concluding remarks

**Conclusions.** This work introduces HOPSE, a *scalable* framework designed to extract and leverage higher-order structural and positional information for *arbitrary combinatorial representations*. Theoretically, HOPSE matches the expressivity of state-of-the-art TNNs while avoiding the HOMP paradigm, thereby substantially reducing the computational cost of training and inference. Moreover, model scaling is linear with dataset size. These claims are supported by experiments on molecular graph benchmarks, as well as expressivity and topological tasks, where both instantiations—**HOPSE-M** and **HOPSE-G**—match or surpass state-of-the-art performance while achieving up to 7x speed-ups over HOMP-based models. By offering a compelling trade-off between scalability and expressivity, this work not only enables broader applicability of TDL but also facilitates the

Table 2: Accuracy on CSL ( $\uparrow$ ).

Model	Mean	Max	Min
MP-GNNs[9]	10.00 $\pm$ 0.00	10.00	10.00
SANN	26.00 $\pm$ 6.83	33.33	20.00
SCCNN	25.33 $\pm$ 7.67	33.33	16.67
GCCN	52.78 $\pm$ 34.28	100.00	3.33
3WLGNN [32]	97.80 $\pm$ 10.92	100.00	30.00
<b>HOPSE-M</b>	<b>100.00 <math>\pm</math> 0.00</b>	100.00	100.00
<b>HOPSE-G</b>	98.00 $\pm$ 4.47	100.00	90.00

integration of higher-order interactions into other areas of deep learning—mirroring the widespread adoption of graph-based methods [47, 44, 24, 25].

**Limitations & future work.** A deeper investigation of HOPSE encodings—along with a comprehensive comparison against alternative methods across diverse domains—lies beyond the scope of this work but remains an important and intriguing direction for future research. Other promising avenues include exploring graph-based strategies for generating higher-order positional and structural encodings, or combining encodings derived from multiple topological domains for enhanced expressivity. Additionally, this work does not address whether integrating the proposed encodings into GNNs, TNNs, or transformer-based architectures leads to substantial improvements across a range of downstream tasks. Finally, and from a more practical standpoint, **HOPSE-G** realization of the framework leverages a pretrained model to extract latent structural and positional features, but it would be interesting to explore if a joint end-to-end training may further enhance performance –even at the cost of additional computational overhead.

## References

- [1] Rubén Ballester, Pablo Hernández-García, Mathilde Papillon, Claudio Battiloro, Nina Miolane, Tolga Birdal, Carles Casacuberta, Sergio Escalera, and Mustafa Hajij. Attending to topological spaces: The cellular transformer. *arXiv preprint arXiv:2405.14094*, 2024.
- [2] Rubén Ballester, Ernst Röell, Daniel Bin Schmid, Mathieu Alain, Sergio Escalera, Carles Casacuberta, and Bastian Rieck. MANTRA: The manifold triangulations assemblage. In *The Thirteenth International Conference on Learning Representations*, 2025. URL <https://openreview.net/forum?id=X6y5CC44HM>.
- [3] Claudio Battiloro, Ege Karaismailoğlu, Mauricio Tec, George Dasoulas, Michelle Audirac, and Francesca Dominici. E (n) equivariant topological neural networks. *The Thirteenth International Conference on Learning Representations (ICLR)*, 2025.
- [4] Federico Battiston, Enrico Amico, Alain Barrat, Ginestra Bianconi, Guilherme Ferraz de Arruda, Benedetta Franceschiello, Iacopo Iacopini, Sonia Kéfi, Vito Latora, Yamir Moreno, et al. The physics of higher-order interactions in complex systems. *Nature Physics*, 17(10):1093–1098, 2021.
- [5] Guillermo Bernández, Lev Telyatnikov, Eduard Alarcón, Albert Cabellos-Aparicio, Pere Barlet-Ros, and Pietro Liò. Topological network traffic compression. In *Proceedings of the 2nd Graph Neural Networking Workshop 2023*, pages 7–12, 2023.
- [6] Guillermo Bernández, Miquel Ferriol-Galmés, Carlos Güemes-Palau, Mathilde Papillon, Pere Barlet-Ros, Albert Cabellos-Aparicio, and Nina Miolane. Ordered topological deep learning: a network modeling case study, 2025. URL <https://arxiv.org/abs/2503.16746>.
- [7] Christian Bick, Elizabeth Gross, Heather A Harrington, and Michael T Schaub. What are higher-order networks? *SIAM Review*, 65(3):686–731, 2023.
- [8] Cristian Bodnar. *Topological deep learning: graphs, complexes, sheaves*. PhD thesis, University of Cambridge, 2023.
- [9] Cristian Bodnar, Fabrizio Frasca, Nina Otter, Yuguang Wang, Pietro Lio, Guido F Montufar, and Michael Bronstein. Weisfeiler and lehman go cellular: Cw networks. *Advances in Neural Information Processing Systems*, 34:2625–2640, 2021.
- [10] Cristian Bodnar, Fabrizio Frasca, Nina Otter, Yuguang Wang, Pietro Lio, Guido F Montufar, and Michael Bronstein. Weisfeiler and Lehman Go Cellular: CW Networks. *Advances in Neural Information Processing Systems*, 34:2625–2640, 2021.
- [11] M.M. Bronstein, J. Bruna, T. Cohen, and P. Veličković. Geometric deep learning: Grids, groups, graphs, geodesics, and gauges. *arXiv preprint arXiv:2104.13478*, 2021.
- [12] Eric Bunch, Qian You, Glenn Fung, and Vikas Singh. Simplicial 2-complex convolutional neural networks. In *TDA & Beyond*, 2020.
- [13] Semih Cantürk, Renming Liu, Olivier Lapointe-Gagné, Vincent Létourneau, Guy Wolf, Dominique Beaini, and Ladislav Rampášek. Graph positional and structural encoder. *arXiv preprint arXiv:2307.07107*, 2023.
- [14] Vijay Prakash Dwivedi, Anh Tuan Luu, Thomas Laurent, Yoshua Bengio, and Xavier Bresson. Graph neural networks with learnable structural and positional representations. *arXiv preprint arXiv:2110.07875*, 2021.
- [15] Vijay Prakash Dwivedi, Ladislav Rampášek, Michael Galkin, Ali Parviz, Guy Wolf, Anh Tuan Luu, and Dominique Beaini. Long range graph benchmark. *Advances in Neural Information Processing Systems*, 35:22326–22340, 2022.
- [16] Vijay Prakash Dwivedi, Chaitanya K. Joshi, Anh Tuan Luu, Thomas Laurent, Yoshua Bengio, and Xavier Bresson. Benchmarking graph neural networks. *Journal of Machine Learning Research*, 24(43):1–48, 2023. URL <http://jmlr.org/papers/v24/22-0567.html>.

[17] Vijay Prakash Dwivedi, Chaitanya K Joshi, Anh Tuan Luu, Thomas Laurent, Yoshua Bengio, and Xavier Bresson. Benchmarking graph neural networks. *Journal of Machine Learning Research*, 24(43):1–48, 2023.

[18] Yifan Feng, Haoxuan You, Zizhao Zhang, Rongrong Ji, and Yue Gao. Hypergraph neural networks. In *Proceedings of the AAAI conference on artificial intelligence*, volume 33, pages 3558–3565, 2019.

[19] Sravanthi Gurugubelli and Sundeep Prabhakar Chepuri. Sann: Simple yet powerful simplicial-aware neural networks. In *The Twelfth International Conference on Learning Representations*, 2023.

[20] Sravanthi Gurugubelli and Sundeep Prabhakar Chepuri. Sann: Simple yet powerful simplicial-aware neural networks. In *The Twelfth International Conference on Learning Representations*, 2024.

[21] M. Hajij, G. Zamzmi, T. Papamarkou, N. Miolane, A. Guzmán-Sáenz, and K. N. Ramamurthy. Higher-order attention networks, 2022.

[22] Mustafa Hajij, Kyle Istvan, and Ghada Zamzmi. Cell complex neural networks. In *Advances in Neural Information Processing Systems Workshop on TDA & Beyond*, 2020.

[23] Mustafa Hajij, Ghada Zamzmi, Theodore Papamarkou, Nina Miolane, Aldo Guzmán-Sáenz, Karthikeyan Natesan Ramamurthy, Tolga Birdal, Tamal Dey, Soham Mukherjee, Shreyas Samaga, Neal Livesay, Robin Walters, Paul Rosen, and Michael Schaub. Topological deep learning: Going beyond graph data. *arXiv preprint arXiv:1906.09068* (v3), 2023.

[24] Kai Han, Yunhe Wang, Jianyuan Guo, Yehui Tang, and Enhua Wu. Vision gnn: An image is worth graph of nodes. *Advances in neural information processing systems*, 35:8291–8303, 2022.

[25] Yan Han, Peihao Wang, Souvik Kundu, Ying Ding, and Zhangyang Wang. Vision hgnn: An image is more than a graph of nodes. In *Proceedings of the IEEE/CVF International Conference on Computer Vision*, pages 19878–19888, 2023.

[26] Ningyuan Teresa Huang and Soledad Villar. A short tutorial on the weisfeiler-lehman test and its variants. In *ICASSP 2021-2021 IEEE International Conference on Acoustics, Speech and Signal Processing (ICASSP)*, pages 8533–8537. IEEE, 2021.

[27] John J Irwin, Teague Sterling, Michael M Mysinger, Erin S Bolstad, and Ryan G Coleman. ZINC: a free tool to discover chemistry for biology. *Journal of Chemical Information and Modeling*, 52(7):1757–1768, 2012.

[28] Kanchan Jha, Sriparna Saha, and Hiteshi Singh. Prediction of protein–protein interaction using graph neural networks. *Scientific Reports*, 12(1):1–12, 2022.

[29] Sandra Kiefer. *Power and limits of the Weisfeiler-Leman algorithm*. PhD thesis, Dissertation, RWTH Aachen University, 2020, 2020.

[30] David Knoke and Song Yang. *Social network analysis*. SAGE publications, 2019.

[31] Liheng Ma, Chen Lin, Derek Lim, Adriana Romero-Soriano, Puneet K Dokania, Mark Coates, Philip Torr, and Ser-Nam Lim. Graph inductive biases in transformers without message passing. In *International Conference on Machine Learning*, pages 23321–23337. PMLR, 2023.

[32] H. Maron, H. Ben-Hamu, H. Serviansky, and Y. Lipman. Provably powerful graph networks. *Advances in Neural Information Processing Systems*, 2019.

[33] Marco Montagna, Simone Scardapane, and Lev Telyatnikov. Topological deep learning with state-space models: A mamba approach for simplicial complexes. *arXiv preprint arXiv:2409.12033*, 2024.

[34] C. Morris, N. M. Kriege, F. Bause, K. Kersting, P. Mutzel, and M. Neumann. Tudataset: A collection of benchmark datasets for learning with graphs. *arXiv preprint arXiv:2007.08663*, 2020.

[35] Christopher Morris, Nils M. Kriege, Franka Bause, Kristian Kersting, Petra Mutzel, and Marion Neumann. TUDataset: a collection of benchmark datasets for learning with graphs. In *ICML Workshop on Graph Representation Learning and Beyond*, 2020.

[36] Ryan Murphy, Balasubramaniam Srinivasan, Vinayak Rao, and Bruno Ribeiro. Relational pooling for graph representations. In *International Conference on Machine Learning*, pages 4663–4673. PMLR, 2019.

[37] Theodore Papamarkou, Tolga Birdal, Michael Bronstein, Gunnar Carlsson, Justin Curry, Yue Gao, Mustafa Hajij, Roland Kwitt, Pietro Liò, Paolo Di Lorenzo, et al. Position paper: Challenges and opportunities in topological deep learning. *arXiv preprint arXiv:2402.08871*, 2024.

[38] Mathilde Papillon, Sophia Sanborn, Mustafa Hajij, and Nina Miolane. Architectures of topological deep learning: A survey on topological neural networks, 2023.

[39] Mathilde Papillon, Guillermo Bernárdez, Claudio Battiloro, and Nina Miolane. Topotune: A framework for generalized combinatorial complex neural networks. *arXiv preprint arXiv:2410.06530*, 2024.

[40] Ladislav Rampášek, Michael Galkin, Vijay Prakash Dwivedi, Anh Tuan Luu, Guy Wolf, and Dominique Beaini. Recipe for a general, powerful, scalable graph transformer. *Advances in Neural Information Processing Systems*, 35:14501–14515, 2022.

[41] Benjamin Sanchez-Lengeling, Emily Reif, Adam Pearce, and Alexander B. Wiltschko. A gentle introduction to graph neural networks. *Distill*, 6(9):e33, 2021.

[42] Lev Telyatnikov, Guillermo Bernardez, Marco Montagna, Pavlo Vasylenko, Ghada Zamzmi, Mustafa Hajij, Michael T Schaub, Nina Miolane, Simone Scardapane, and Theodore Papamarkou. Topobench: A framework for benchmarking topological deep learning. *arXiv preprint arXiv:2406.06642*, 2024.

[43] Haorui Wang, Haoteng Yin, Muhan Zhang, and Pan Li. Equivariant and stable positional encoding for more powerful graph neural networks. *arXiv preprint arXiv:2203.00199*, 2022.

[44] Zhe Wang, Sheng Zhou, Jiawei Chen, Zhen Zhang, Binbin Hu, Yan Feng, Chun Chen, and Can Wang. Dynamic graph transformer with correlated spatial-temporal positional encoding. In *Proceedings of the Eighteenth ACM International Conference on Web Search and Data Mining*, pages 60–69, 2025.

[45] Amaury Wei and Olga Fink. Physics meets topology: Physics-informed topological neural networks for learning rigid body dynamics, 2024. URL <https://arxiv.org/abs/2411.11467>.

[46] Jie Zhou, Ganqu Cui, Shengding Hu, Zhengyan Zhang, Cheng Yang, Zhiyuan Liu, Lifeng Wang, Changcheng Li, and Maosong Sun. Graph neural networks: A review of methods and applications. *AI Open*, 1:57–81, 2020.

[47] Yixiao Zhou, Ruiqi Jia, Hongxiang Lin, Hefeng Quan, Yumeng Zhao, and Xiaoqing Lyu. Improving graph matching with positional reconstruction encoder-decoder network. *Advances in Neural Information Processing Systems*, 36:34557–34569, 2023.

## A Extended background

### A.1 Topological domains

This section draws primarily from Appendix A of Telyatnikov et al. [42]. It begins with the fundamental concept of featured graphs, which forms the basis for understanding more intricate structures. Then it proceeds to explore higher-order domains — including simplicial complexes, cell complexes, and combinatorial complexes — each providing distinct capabilities for representing various types of relationships and hierarchies within data.

**Definition A.1.** Let  $\mathcal{G} = (V, E)$  be a graph, with node set  $V$  and edge set  $E$ . A featured graph is a tuple  $\mathcal{G}_F = (V, E, F_V, F_E)$ , where  $F_V : V \rightarrow \mathbb{R}^{d_v}$  is a function that maps each node to a feature vector in  $\mathbb{R}^{d_v}$  and  $F_E : E \rightarrow \mathbb{R}^{d_e}$  is a function that maps each edge to a feature vector in  $\mathbb{R}^{d_e}$ .

A topological domain is a graph generalization that captures pairwise and higher-order relationships between entities [7, 4]. When working with topological domains, two key properties come into play: set-type relations and hierarchical structures represented by rank functions [23, 38].

**Definition A.2** (Set-type relation). A relation in a topological domain is called a *set-type relation* if another relation in the domain does not imply its existence.

**Definition A.3** (Rank function). A *rank function* on a higher-order domain  $\mathcal{X}$  is an order-preserving function  $rk : \mathcal{X} \rightarrow \mathbb{Z}_{\geq 0}$  such that  $x \subseteq y$  implies  $rk(x) \leq rk(y)$  for all  $x, y \in \mathcal{X}$ .

Set-type relations emphasize the independence of connections within a domain, allowing for flexible representation of complex interactions. In contrast, rank functions introduce a hierarchical (also called part-whole) organization that facilitates the representation and analysis of nested relationships.

**Simplicial complexes.** Simplicial complexes extend graphs by incorporating hierarchical part-whole relationships through the multi-scale construction of cells. In this structure, nodes correspond to rank 0-cells, which can be combined to form edges (rank 1-cells). Edges can then be grouped to form faces (rank 2 cells), and faces can be combined to create volumes (rank 3-cells), continuing in this manner. Consequently, the faces of a simplicial complex are triangles, volumes are tetrahedra, and higher-dimensional cells follow the same pattern. A key feature of simplicial complexes is their strict hierarchical structure, where each  $k$ -dimensional simplex is composed of  $(k - 1)$ -dimensional simplices, reinforcing a strong sense of hierarchy across all levels.

**Definition A.4** (Simplicial Complex). A *simplicial complex* (*SC*) in a non-empty set  $S$  is a pair  $SC = (S, \mathcal{X})$ , where  $\mathcal{X} \subset \mathcal{P}(S) \setminus \{\emptyset\}$  satisfies: if  $x \in SC$  and  $y \subseteq x$ , then  $y \in SC$ . The elements of  $\mathcal{X}$  are called *simplices*.

*Example 1* (3D Surface Meshes). 3D models of objects, such as those used in computer graphics or for representing anatomical structures, are often constructed using triangular meshes. These meshes naturally form simplicial complexes, where the vertices of the triangles are 0-simplices, the edges are 1-simplices, and the triangular faces themselves are 2-simplices.

**Cell complexes** Cell complexes provide a hierarchical interior-to-boundary structure, offering clear topological and geometric interpretations, but they are not based on set-type relations. Unlike simplicial complexes, cell complexes are not limited to simplexes; faces can involve more than three nodes, allowing for a more flexible representation. This increased flexibility grants cell complexes greater expressivity compared to simplicial complexes [10, 8].

**Definition A.5** (Cell complex). A *regular cell complex* is a topological space  $S$  partitioned into subspaces (cells)  $\{x_\alpha\}_{\alpha \in P_S}$ , where  $P_S$  is an index set, satisfying:

1.  $S = \bigcup_{\alpha \in P_S} \text{int}(x_\alpha)$ , where  $\text{int}(x)$  denotes the interior of cell  $x$ .
2. For each  $\alpha \in P_S$ , there exists a homeomorphism  $\psi_\alpha$  (*attaching map*) from  $x_\alpha$  to  $\mathbb{R}^{n_\alpha}$  for some  $n_\alpha \in \mathbb{N}$ . The integer  $n_\alpha$  is the *dimension* of cell  $x_\alpha$ .
3. For each cell  $x_\alpha$ , the boundary  $\partial x_\alpha$  is a union of finitely many cells of strictly lower dimension.

*Example 2* (Molecular structures.). Molecules admit natural representations as cell complexes by considering atoms as nodes (i.e., cells of rank zero), bonds as edges (i.e., cells of rank one), and rings as faces (i.e., cells of rank two).

**Combinatorial complexes.** Combinatorial complexes combine hierarchical structure with set-type relations, enabling a flexible yet comprehensive representation of higher-order networks.

**Definition A.6** (Combinatorial complex). A *combinatorial complex* (CC) is a triple  $(\mathcal{V}, \mathcal{C}, k)$  consisting of a set  $\mathcal{V}$ , a subset  $\mathcal{C} \subset \mathcal{P}(\mathcal{V}) \setminus \{\emptyset\}$ , and a function  $rk: \mathcal{C} \rightarrow \mathbb{Z}_{\geq 0}$  satisfying:

1. For all  $v \in \mathcal{V}$ ,  $\{v\} \in \mathcal{C}$  and  $rk(v) = 0$ .
2. The function  $rk$  is order-preserving: if  $x, y \in \mathcal{C}$  with  $x \subseteq y$ , then  $rk(x) \leq rk(y)$ .

*Example 3* (Geospatial structures.). Geospatial data, comprised of grid points (0-cells), road polylines (1-cells), and census tract polygons (2-cells), can be effectively represented using combinatorial complexes. A visual example is provided in Figure 2 (Right) of Battiloro et al. [3].

**Featured topological domains.** A featured graph is a graph whose nodes or edges are equipped with feature functions [41]. Similarly, each topological element (e.g., simplex or cell) can carry feature vectors to represent some information.

**Definition A.7** (Featured topological domain). A *featured topological domain* is a pair  $(\mathcal{X}, F)$ , where  $\mathcal{X}$  is a topological domain and  $F = \{F_i\}_{i \geq 0}$  is a collection of feature functions. Each function  $F_i$  maps the  $i$ -dimensional elements of  $\mathcal{X}$ , denoted  $\mathcal{X}_i$ , to a feature space  $\mathbb{R}^{k_i}$ :

$$F_i: \mathcal{X}_i \rightarrow \mathbb{R}^{k_i}.$$

## A.2 Neighborhood functions and augmented Hasse graphs

Discrete topological domains are equipped with a notion of neighborhood among cells that confers on them a topological structure; this section revisits the main neighborhood-related concepts in the general combinatorial complex case.

**Definition A.8** (Neighborhood function). Given a combinatorial complex  $\mathcal{T} = (\mathcal{V}, \mathcal{C}, k)$ , a neighborhood  $\mathcal{N}: \mathcal{C} \rightarrow \mathcal{P}(\mathcal{C})$  on a combinatorial complex is a function that assigns to each cell  $\sigma \in \mathcal{C}$  a collection of *neighbor cells*  $\mathcal{N}(\sigma) \subset \mathcal{C} \cup \emptyset$ .

Each neighborhood can be used to create a Strictly Augmented Hasse graph.

**Definition A.9** (Strictly augmented Hasse graph). Each particular neighborhood  $\mathcal{N}$  induces a strictly augmented Hasse graph  $\mathcal{G}_{\mathcal{N}} = (\mathcal{C}_{\mathcal{N}}, \mathcal{E}_{\mathcal{N}})$  on  $\mathcal{T}$  [39, 23], defined as the directed graph whose nodes and edges are given, respectively, by  $\mathcal{C}_{\mathcal{N}} = \{\sigma \in \mathcal{C} \mid \mathcal{N}(\sigma) \neq \emptyset\}$  and  $\mathcal{E}_{\mathcal{N}} = \{(\tau, \sigma) \mid \tau \in \mathcal{N}(\sigma)\}$ .

Examples of neighborhood functions are incidences (connecting cells with different ranks) and adjacencies (connecting cells with the same rank), although other neighborhoods can be defined for specific tasks [3]. More in detail, given a combinatorial complex  $\mathcal{T}$ :

**Definition A.10.** (Incidences) The incidence neighborhood of a  $t$ -cell  $\sigma \in \mathcal{T}$  with respect to a rank  $s$  is defined as

$$\mathcal{I}_{s \rightarrow t}(\sigma) = \begin{cases} \{\tau \in \mathcal{C} \mid rk(\tau) = s, \sigma \subset \tau\} & \text{if } t < s; \\ \{\tau \in \mathcal{C} \mid rk(\tau) = s, \tau \subset \sigma\} & \text{if } t > s. \end{cases} \quad (7)$$

A  $s$ -cell  $\tau \in \mathcal{T}$  is said to be co-incident of  $\sigma$  if it contains  $\sigma$  and  $s > t$ ; analogously, a  $s$ -cell  $\tau \in \mathcal{T}$  is incident of  $\sigma$  if it is contained by  $\sigma$  and  $s < t$ .

Incidences in turn induce adjacency neighborhoods of cells of the same rank as follows:

**Definition A.11** (Adjacencies). The adjacency neighborhood of a  $t$ -cell  $\sigma \in \mathcal{T}$  with respect to a rank  $s$  is defined as

$$\mathcal{A}_{s,t}(\sigma) = \{\tau \in \mathcal{C} \mid rk(\tau) = t, \mathcal{I}_{s \rightarrow t}(\sigma) \cap \mathcal{I}_{s \rightarrow t}(\tau) \neq \emptyset\} \quad (8)$$

In this case, two  $t$ -cells  $\sigma$  and  $\tau$  are said to be adjacent if they are both contained in a  $s$ -cell  $\delta \in \mathcal{T}$ .

## B Counting neighborhoods and message passing routes

This section provides a detailed discussion of two key concepts in Topological Deep Learning: *expanded neighborhoods* and *the combinatorial explosion of message passing routes*. This discussion, while emphasizing the expressive power of combinatorial representations, highlights the challenges they pose when scaling to real-world problems.

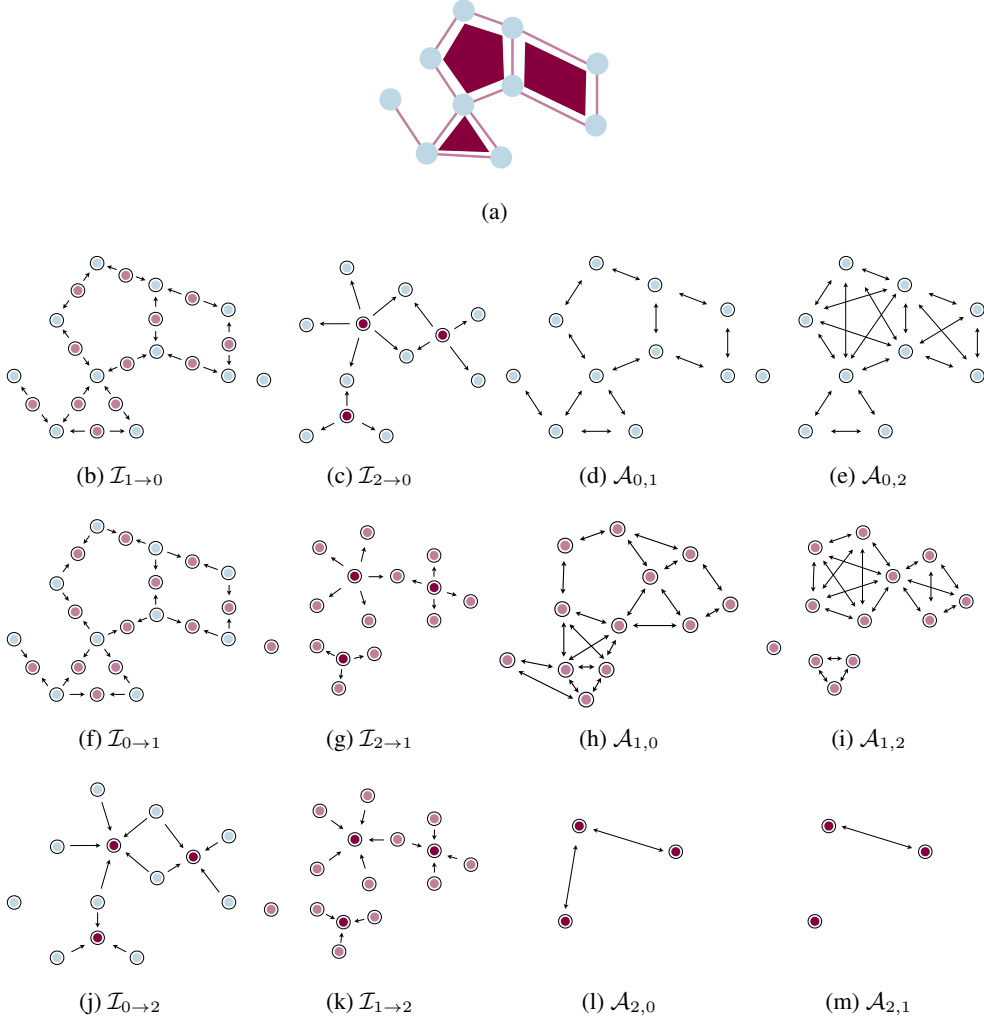


Figure 3: Illustration of a combinatorial complex (top) and different neighborhood types, grouped by the target entity: nodes (second row), edges (third row), and faces (bottom row).

### B.1 Neighborhood Types in Combinatorial Complexes

Combinatorial representations allow for a variety of neighborhood types, depending on how cells of different ranks interact. For a 2-dimensional combinatorial complex (with 0-, 1-, and 2-cells), Figure 3 illustrates all possible neighborhood types. These relations can be grouped into two main groups:

- **Incidence Relations:**
  - (b)  $\mathcal{I}_{1 \rightarrow 0}$ : edges  $\rightarrow$  nodes
  - (c)  $\mathcal{I}_{2 \rightarrow 0}$ : faces  $\rightarrow$  nodes
  - (f)  $\mathcal{I}_{0 \rightarrow 1}$ : nodes  $\rightarrow$  edges
  - (g)  $\mathcal{I}_{2 \rightarrow 1}$ : faces  $\rightarrow$  edges
  - (j)  $\mathcal{I}_{0 \rightarrow 2}$ : nodes  $\rightarrow$  faces
  - (k)  $\mathcal{I}_{1 \rightarrow 2}$ : edges  $\rightarrow$  faces
- **Adjacency Relations:**
  - (d)  $\mathcal{A}_{0,1}$ : nodes  $\rightarrow$  nodes (via edges)
  - (e)  $\mathcal{A}_{0,2}$ : nodes  $\rightarrow$  nodes (via faces)
  - (h)  $\mathcal{A}_{1,0}$ : edges  $\rightarrow$  edges (via nodes)

- (i)  $\mathcal{A}_{1,2}$ : edges  $\rightarrow$  edges (via faces)
- (l)  $\mathcal{A}_{2,0}$ : faces  $\rightarrow$  faces (via nodes)
- (m)  $\mathcal{A}_{2,1}$ : faces  $\rightarrow$  faces (via edges)

## B.2 Counting neighborhoods

The combinatorial complex depicted in Figure 3 has rank  $R = \dim(\mathcal{T}) = 2$ , which results in 12 *distinct neighborhood types*. These neighborhoods can be divided into the two categories from above: (i) incidence relations and (ii) adjacency relations.

Under these assumptions, the number of incidence relations is  $|I| = (R + 1)R$ , as each of the  $R + 1$  ranks can be connected to any of the remaining  $R$  ranks. Similarly, each rank gives rise to  $R$  possible adjacency relations (each defined through a different intermediary rank), also resulting in  $|A| = (R + 1)R$ . Combining these yields a total of

$$|\mathcal{N}_{\mathcal{T}}| = 2(R + 1)R$$

distinct neighborhood types. For the example in Figure 3, where  $R = 2$ , this formula recovers the 12 neighborhoods observed.

## B.3 Message passing routes

The number of neighborhoods increases quadratically with the maximum rank, which may initially seem manageable, especially since most practical datasets involve low-rank structures (e.g.,  $R = 2$  or  $R = 3$ ). However, the true combinatorial complexity arises when considering how these neighborhoods can be composed. To formalize this notion, the following definition is introduced.

**Definition B.1** (Message passing route). A message passing route is an ordered set of neighborhoods that a model uses to propagate information across a data structure.

Information may flow *intra-rank*, through adjacency relations, or *inter-rank*, through incidence relations. For example, a network might use the message passing route  $[\mathcal{I}_{2 \rightarrow 1}, \mathcal{I}_{1 \rightarrow 0}, \mathcal{I}_{0 \rightarrow 2}, \mathcal{A}_{0,1}]$  to transmit information from faces to edges, then from edges to nodes, from nodes back to faces, and finally between nodes connected by an edge.

Given a fixed combinatorial complex, the number of possible message passing routes is infinite, since any sequence can reuse the same neighborhood relations and grow to arbitrary length. In what follows, the analysis is restricted to a subset of message passing routes that are particularly relevant for the design of higher-order neural architectures.

**Definition B.2** (Minimal message passing route). A minimal message passing route is a message passing route of minimal length that updates all ranks in a higher-order representation at least once. Furthermore, it ensures that, after a sufficient number of message passing steps, the representation of each rank depends on all other ranks.

Minimal routes are of particular interest, as they guarantee full interdependence between all cells—a desirable property for expressive models. Moreover, minimal length implies simplicity in design, yielding the most compact routes that preserve this full dependency. For instance, the previously introduced route  $[\mathcal{I}_{2 \rightarrow 1}, \mathcal{I}_{1 \rightarrow 0}, \mathcal{I}_{0 \rightarrow 2}, \mathcal{A}_{0,1}]$  can be transformed into a minimal message passing route by removing the adjacency  $\mathcal{A}_{0,1}$ . In this reduced route, information from all cells becomes accessible to all others within two message passing steps. In fact, consider the case of 0-cells: after the first step, they depend on 1-cells; after the second step, since 1-cells now incorporate information from 2-cells, the 0-cells become indirectly connected to them as well.

By definition, minimal message passing routes rely exclusively on incidence relations, as adjacencies do not propagate information inter-rank. Since each incidence targets a specific rank, and every rank must be updated once, minimal routes necessarily have length  $R + 1$ . To enumerate all possible minimal routes, consider the set of ranks  $T = \{0, 1, \dots, R\}$ , of size  $R + 1$ . There are  $(R + 1)!$  distinct permutations of these ranks, each defining a unique order in which the ranks are updated. Given such a permutation  $\{r_0, r_1, \dots, r_R\}$ , a corresponding minimal message passing route can be constructed by selecting the sequence of incidence relations  $\mathcal{I}_{r_{j-1} \rightarrow r_j}$  for  $j = 1, \dots, R$ , and closing the cycle with  $\mathcal{I}_{r_R \rightarrow r_0}$ . This construction yields exactly one valid minimal route per permutation, resulting in a total of  $N = (R + 1)!$  such routes. In the case of graphs, where  $R = 1$ , this results in exactly two minimal message passing routes—an intuitively expected outcome.

#### B.4 Beyond minimal routes: including adjacencies

Minimal message passing routes represent only a small subset of the possible routes that can be constructed using the full set of neighborhoods in a combinatorial complex. A natural extension involves augmenting these minimal routes with adjacency operations—a common practice in many TDL architectures. For simplicity, the analysis here is restricted to the case where adjacencies are applied strictly after all incidence relations.

As previously discussed, for a given rank  $r$ , there are  $R$  possible adjacency relations of the form  $\mathcal{A}_{r,x}$ . Since adjacencies operate intra-rank, they do not affect inter-rank dependencies and merely update the representation of the corresponding rank. As a consequence, the order in which these adjacencies are applied does not impact the outcome of the message passing route. For example, applying  $\mathcal{A}_{0,0}$  followed by  $\mathcal{A}_{1,1}$  produces the same result as applying them in reverse order.

Given that each of the  $R + 1$  ranks can be updated with any of their  $R$  possible adjacencies, there are  $(R + 1)^R$  combinations of adjacency updates. When combined with the  $(R + 1)!$  minimal incidence-based routes, the total number of extended message passing routes becomes  $\hat{N} = (R + 1)! \cdot (R + 1)^R$ .

## C Proofs

Before proving Theorem 4.1, the following paragraphs show that HOPSE is at least as powerful as the WL test. Although this is a weaker result than the one from Theorem 4.1, the proof is more intuitive, making it a valuable tool to understand the HOPSE model.

First, a beneficial result from Gurugubelli and Chepuri [20] regarding the WL test is reported.

**Lemma C.1.** *For a graph  $\mathcal{G} = (\mathcal{V}, \mathcal{E})$ , the update of WL coloring of a node  $\sigma \in \mathcal{V}$  at iteration  $K$  can be represented by the following equation*

$$c_{\sigma}^{(K)} = \phi \left( c_{\sigma}^{(0)}, \{ \{ c_{\tau}^{(0)}, \forall \tau \in \{ \mathcal{U}^{(1)}(\sigma), \dots, \mathcal{U}^{(K)}(\sigma) \} \} \} \right), \quad (9)$$

where  $\phi(\cdot)$  is some injective function and  $\mathcal{U}^{(k)}(\sigma)$  denotes the set of upper adjacent  $t$ -hop neighbors of node  $\sigma$ .

Using this lemma, the following theorem can now be tackled.

**Theorem C.2.** *HOPSE is at least as powerful as the WL test in distinguishing non-isomorphic graphs if the functions  $\varepsilon_r(\cdot)$ ,  $g_k(\cdot)$ ,  $\psi_k(\cdot)$ ,  $f_{r,k}(\cdot)$ , and  $\Theta_r(\cdot)$  are injective for all  $k \in 1, \dots, K$  and for all  $r \in 0, \dots, R$ .*

*Proof.* Let  $\mathcal{T}_1$  and  $\mathcal{T}_2$  be two graphs. By considering their nodes as zero rank cells and their edges as rank-1 cells, they can be considered as CC without loss of generalization. Given two nodes (zero rank cells)  $\sigma_1 \in \mathcal{T}_1$  and  $\sigma_2 \in \mathcal{T}_2$  let  $c_{\sigma_1}^{(K)}, c_{\sigma_2}^{(K)}$  be the WL coloring of the two nodes after  $K$  steps of the WL algorithm, and  $h_{\sigma_1}^{(K)}$  and  $h_{\sigma_2}^{(K)}$  be the embeddings obtained with HOPSE using a set of neighborhoods  $\{\mathcal{N}_1, \dots, \mathcal{N}_T\}$ . Showing that for all graphs  $\mathcal{T}_1$  and  $\mathcal{T}_2$  and for all nodes  $\sigma_1$  and  $\sigma_2$ , there exists a version of HOPSE such that  $h_{\sigma_1}^{(K)} = h_{\sigma_2}^{(K)}$  implies  $c_{\sigma_1}^{(K)} = c_{\sigma_2}^{(K)}$  proves that HOPSE is at least as powerful as the WL isomorphism test. This is because it would mean that the WL test fails to assign different embeddings whenever HOPSE fails.

As the focus is solely on the embeddings of the nodes in the considered graphs, the target rank is fixed to  $r_k = 0$ , which is omitted in the remainder of the proof for clarity. Furthermore, since only neighborhoods  $\mathcal{N}_k$  with target rank 0 are relevant, the proof is restricted to the case  $\mathcal{N}_k = \mathcal{U}^{(k)}$  for  $k \in 1, \dots, K$ , where  $\mathcal{U}^{(k)}$  denotes the upper adjacent  $k$ -hop neighborhood.

Without loss of generality, the analysis can be restricted to *strictly augmented multi-attributed Hasse graphs* defined in Section 4 of the form  $\mathcal{J}_{\mathcal{N}} = (\mathcal{C}_{\mathcal{N}}, \mathcal{E}_{\mathcal{N}}, \mathcal{F}_{\mathcal{N}})$ , where  $\mathcal{F}_{\mathcal{N}} = \mathcal{F}$  for all  $\mathcal{N} \in N^{\rightarrow 0}$ , and  $\mathcal{F}$  denotes the initial node features of the graph. As only a single feature type is considered, the index  $k = 0$  is omitted in the remainder of the proof for clarity.

For any node  $\sigma$ , by combining equation 4 to equation 5 the HOPSE embeddings can be written as

$$h_{\sigma}^{(K)} = \Theta \left( \varepsilon(\mathbf{Z}), \{ f \left( \psi \left( \{ g(\sigma, \mathcal{J}_{\mathcal{N}_j}) \mid \mathcal{N}_j \in N^{\rightarrow 0} \} \right) \right) \} \right). \quad (10)$$

Since  $g(\mathcal{J}_N)$  is the function that creates the encodings for all target cells in the graph by creating a row for each cell,  $g(\sigma, \mathcal{J}_N)$  is defined as the row-wise version of  $g(\mathcal{J}_N)$ .

The functions  $g(\sigma, \mathcal{J}_N)$  can be any injective functions, but by considering only functions that depend on the 1-hop neighbors of  $\sigma$  in the corresponding Hasse graph, it is immediate to see that  $g(\sigma, \mathcal{J}_{U_j}) = \xi(\{\mathcal{F}[\tau] \mid \forall \tau \in \mathcal{U}^{(j)}(\sigma)\})$ , given that  $\mathcal{N}_j = \mathcal{U}^{(j)}$ . Since by hypothesis  $g(\cdot)$  is injective, also  $\xi(\cdot)$  is. Since  $\varepsilon(\cdot)$  is also injective by hypothesis equation 10 can be rewritten as

$$\begin{aligned} h_\sigma^{(K)} &= \hat{\Theta} \left( c_\sigma^{(0)}, \{c_\tau^{(0)}, \forall \tau \in \mathcal{U}^{(1)}(\sigma)\}, \dots, \{c_\tau^{(0)}, \forall \tau \in \mathcal{U}^{(K)}(\sigma)\} \right) = \\ &= \hat{\Theta} \left( c_\sigma^{(0)}, \{c_\tau^{(0)}, \forall \tau \in \{\mathcal{U}^{(1)}(\sigma), \dots, \mathcal{U}^{(K)}(\sigma)\}\} \right), \end{aligned} \quad (11)$$

where the fact that  $c_\sigma^{(0)} = \mathbf{Z}$  was used, which means that for the WL coloring algorithm the nodes' features are the initial features. Also, since the functions  $\Theta(\cdot)$ ,  $f(\cdot)$ ,  $\psi(\cdot)$ , and  $\xi(\cdot)$  are injective,  $\hat{\Theta}(\cdot)$  is also injective since it is a composition of injective functions.

Since  $\hat{\Theta}$  is injective  $h_{\sigma_1}^{(K)} = h_{\sigma_2}^{(K)}$  implies that the arguments of  $\hat{\Theta}$  are equal. But those arguments are the exact arguments for the WL colorings of nodes  $\sigma_1$  and  $\sigma_2$  reported in equation 9, which means that  $h_{\sigma_1}^{(K)} = h_{\sigma_2}^{(K)}$  implies  $c_{\sigma_1}^{(K)} = c_{\sigma_2}^{(K)}$ . As discussed previously, this implies that HOPSE is at least as powerful as the WL test.  $\square$

The definition of the CCWL test, which generalizes the WL test to combinatorial complexes, is taken from [39].

**Definition C.3** (The CC Weisfeiler-Leman (CCWL) test on labeled combinatorial complexes). Let  $(\mathcal{T}, F)$  be a labelled combinatorial complex. Let  $\mathcal{N}$  be a neighborhood on  $\mathcal{C}$ . The scheme proceeds as follows:

- Initialization: Cells  $\sigma$  are initialized with the labels given by  $F$ , i.e.: for all  $\sigma \in \mathcal{C}$ :  $c_{\sigma, F}^{(0)} = F(\sigma)$ .
- Refinement: Given colors of cells at iteration  $k$ , the refinement step computes the color of cell  $\sigma$  at the next iteration  $c_{\sigma, F}^{(k+1)}$  using a perfect HASH function as follows:

$$\begin{aligned} c_{\mathcal{N}}^{(k)}(\sigma) &= \{c_{\tau, F}^{(k)} \mid \forall \tau \in \mathcal{N}(\sigma)\}, \\ c_{\sigma, F}^{(k+1)} &= \text{HASH} \left( c_{\sigma, F}^{(k)}, c_{\mathcal{N}}^{(k)}(\sigma) \right). \end{aligned} \quad (12)$$

- Termination: The algorithm stops when an iteration leaves the coloring unchanged.

To show that HOPSE is more powerful than the CCWL test, the following lemma is proven first.

**Lemma C.4.** *For a combinatorial complex  $(\mathcal{T}, F)$  the update of CCWL coloring of a cell  $\sigma \in \mathcal{C}$  at iteration  $T$  can be represented as the following equation*

$$c_\sigma^{(K)} = \phi \left( c_\sigma^{(0)}, \{c_\tau^{(0)}, \forall \tau \in \{\mathcal{N}^{(1)}(\sigma), \dots, \mathcal{N}^{(K)}(\sigma)\}\} \right), \quad (13)$$

where  $\phi(\cdot)$  is some injective function, and  $\mathcal{N}^{(k)}$  denotes the  $k$ -hops version of the neighborhood  $\mathcal{N}$ .

*Proof.* The proof is by induction. For  $k = 0$ , the equation holds trivially, since the initial coloring for cell  $\sigma$  is  $c_\sigma^{(0)}$ . Assuming that the  $k - 1$  update is true

$$c_\sigma^{(t-1)} = \phi_0 \left( c_\sigma^{(0)}, \{c_\tau^{(0)}, \forall \tau \in \{\mathcal{N}^{(1)}(\sigma), \dots, \mathcal{N}^{(t-1)}(\sigma)\}\} \right).$$

By substituting this in equation 12 the  $k$  update can be written as

$$\begin{aligned} c_\sigma^{(k)} &= \text{HASH} \left( \phi_0 \left( c_\sigma^{(0)}, \{c_\tau^{(0)}, \forall \tau \in \{\mathcal{N}^{(1)}(\sigma), \dots, \mathcal{N}^{(t-1)}(\sigma)\}\} \right), \right. \\ &\quad \left. \{\phi_0 \left( c_v^{(0)}, \{c_\tau^{(0)}, \forall \tau \in \{\mathcal{N}^{(1)}(\sigma), \dots, \mathcal{N}^{(t-1)}(\sigma)\}\} \right), \forall v \in \mathcal{N}^{(1)}(\sigma)\} \right). \end{aligned}$$

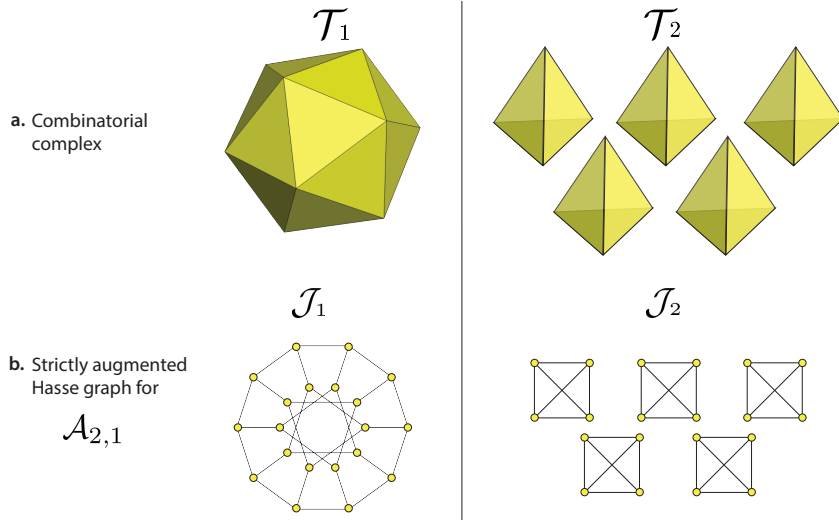


Figure 4: **a.** Two combinatorial complexes with nodes, edges, and faces.  $\mathcal{T}_1$  is a icosahedron while  $\mathcal{T}_2$  is composed of five tetrahedrons. **b.** Their respective Hasse graphs given the choice of the neighborhood  $\mathcal{A}_{2,1}$ , which connects faces that share an edge. Image adapted from [39].

Now, since HASH and  $\phi_0$  are injective functions, it follows that

$$\begin{aligned}
c_{\sigma}^{(k)} &= \phi\left(c_{\sigma}^{(0)}, \{c_{\tau}^{(0)}, \forall \tau \in \{\mathcal{N}^{(1)}(\sigma), \dots, \mathcal{N}^{(t-1)}(\sigma)\}\}, \right. \\
&\quad \left. \{c_v^{(0)}, \{c_{\tau}^{(0)}, \forall \tau \in \{\mathcal{N}^{(1)}(\sigma), \dots, \mathcal{N}^{(t-1)}(\sigma)\}\}, \forall v \in \mathcal{N}^{(1)}(\sigma)\} \right) \\
&= \phi\left(c_{\sigma}^{(0)}, \{c_{\tau}^{(0)}, \forall \tau \in \{\mathcal{N}^{(1)}(\sigma), \dots, \mathcal{N}^{(t-1)}(\sigma)\}\}, \{c_{\tau}^{(0)}, \forall \tau \in \{\mathcal{N}^{(1)}(\sigma), \dots, \mathcal{N}^{(k)}(\sigma)\}\} \right) \\
&= \phi\left(c_{\sigma}^{(0)}, \{c_{\tau}^{(0)}, \forall \tau \in \{\mathcal{N}^{(1)}(\sigma), \dots, \mathcal{N}^{(k)}(\sigma)\}\} \right)
\end{aligned}$$

This is the result needed, so the theorem is proven by induction.  $\square$

This result is the combinatorial complex equivalent of Lemma C.1, and it can now be used to prove the following theorem.

**Theorem C.5.** *HOPSE is at least as powerful as the CCWL test in distinguishing non-isomorphic combinatorial complexes if the functions  $\varepsilon_r(\cdot)$ ,  $g_k(\cdot)$ ,  $\psi_k(\cdot)$ ,  $f_{r,k}(\cdot)$ , and  $\Theta_r(\cdot)$  are injective for all  $k \in 1, \dots, K$  and for all  $i \in 0, \dots, R$ .*

*Proof.* Given that Lemma C.4 is equivalent to Lemma C.1 with  $\mathcal{N}_i = \mathcal{N}^{(i)}$  for  $i \in 0, \dots, K$ , this proof follows the same steps as the proof for Theorem C.2.  $\square$

Now the two main theorems of the paper can be proven.

**Theorem** (Theorem 4.1). *HOPSE is more powerful than the CCWL test in distinguishing non-isomorphic combinatorial complexes if the functions  $\varepsilon_r(\cdot)$ ,  $g_k(\cdot)$ ,  $\psi_k(\cdot)$ ,  $f_{r,k}(\cdot)$ , and  $\Theta_r(\cdot)$  are injective for all  $k \in 1, \dots, K$  and for all  $r \in 0, \dots, R$ .*

*Proof.* Since HOPSE matches the expressive power of CCWL, as established in Theorem C.5, to prove this theorem is sufficient to present a case in which two combinatorial complexes are indistinguishable by the CCWL test but are successfully distinguished by the HOPSE algorithm. The example in Figure 4 illustrates two such CCs. Using the neighborhood  $\mathcal{A}_{2,1}$  (the faces are adjacent if they share an edge), the corresponding Hasse graphs  $\mathcal{J}_1$  and  $\mathcal{J}_2$  are constructed, both of which are 3-regular. It is known that the WL test cannot distinguish between regular graphs of the same degree [29]. According to Proposition B.11 in [39], the CCWL test on these CCs is equivalent to the WL test on  $\mathcal{J}_1$  and  $\mathcal{J}_2$ , and thus also fails to distinguish them. However, the HOPSE algorithm can separate

the two cases. In fact, by choosing the function  $g_1(\cdot)$  to return the size of the connected component to which a node belongs, the difference between the two HOPSE encodings is apparent.  $\square$

**Theorem** (Theorem 4.2). *HOPSE is cell permutation equivariant if the functions  $\varepsilon_r(\cdot)$ ,  $g_k(\cdot)$ ,  $\psi_k(\cdot)$ ,  $f_{r,k}(\cdot)$ , and  $\Theta_r(\cdot)$  are cell permutation equivariant for all  $k \in 1, \dots, K$  and all  $r \in 0, \dots, R$ .*

*Proof.* To demonstrate that HOPSE is cell permutation equivariant, it suffices to show that the composition of permutation equivariant functions remains permutation equivariant. Since, by assumption, all functions that compose HOPSE are permutation equivariant, the result follows directly. Let  $\pi(\cdot)$  be the permutation operator. Then  $p(\cdot)$  is permutation equivariant if  $\pi(p(\cdot)) = p(\pi(\cdot))$ . Given two permutaiton equivariant functions  $p(\cdot)$  and  $q(\cdot)$  their composition  $r(\cdot) = (p \circ q)(\cdot)$  is also permutation equivariant:

$$r(\pi(\cdot)) = (p \circ q)(\pi(\cdot)) = p(q(\pi(\cdot))) = p(\pi(q(\cdot))) = \pi(p(q(\cdot))) = \pi(r(\cdot)).$$

$\square$

## D Framework realization

This section contains an in-depth description of the algorithmic procedure for extracting structural and positional information according two the proposed realizations **HOPSE-M** and **HOPSE-G**. Complementary to Section 4.3 the following is an in-depth explanation of the procedure for computing the positional and structural encodings of both realizations.

The first step in the pipeline is the definition of the family of functions  $(g_0, \dots, g_K)$  and the same target aggregations  $\psi_k(\cdot)$ . Both the variations have a different way of calculating the output embeddings so both of the cases are shown.

### D.1 Precomputation of HOPSE-M

In this case four hand-picked structural and positional encodings were used. Let  $\mathcal{G} = (V, E)$  be an undirected graph with  $|V| = n$  nodes. The individual channels  $g_k(\mathcal{G})$  are defined as follows:

1.  $g_1(\cdot) = \text{LapPE}_i = [\phi_1, \dots, \phi_i] \in \mathbb{R}^{n \times i}$ , the first  $i$  nontrivial eigenvectors of the graph Laplacian (up to frequency  $i$ ).
2.  $g_2(\cdot) = \text{RWSE}_K \in \mathbb{R}^{n \times K}$ , the Random Walk Structural Encodings, obtained by stacking the diagonal entries of the  $t$ -step random-walk transition matrices for  $t = 1, \dots, K$  (here  $K = 60$ ).
3.  $g_3(\cdot) = \text{HKdiagSE}_K \in \mathbb{R}^{n \times K}$ , the Heat Kernel Diagonal Structural Encodings, given by  $[\exp(-\lambda_j t)]_{j=1, \dots, n; t=1, \dots, K}$  for the Laplacian eigenvalues  $\{\lambda_j\}$ .
4.  $g_4(\cdot) = \text{ElstaticPE} \in \mathbb{R}^{n \times d_4}$ , the Electrostatic Potential Positional Encodings, computed by solving the discrete Poisson equation on  $\mathcal{G}$  with suitable boundary conditions.

Importantly, since each  $g_k$  depends only on the adjacency structure of  $\mathcal{G}$ , none of these channels requires access to any node feature vectors. For more indepth explanation of each PS encoding, see [13].

### D.2 Precomputation of HOPSE-G

As mentioned previously, this method relies on the use of GPSE. This is a pre-trained graph PSE presented by Cantürk et al. [13]. The pre-trained component consists of a GNN model pre-trained on a set of different datasets: ZINC, MolPCBA, GEOM, PCQM4Mv2 and ChEMBL. During the pre-training, a combination of losses targeting positional and structural properties is used to learn a latent representation of them.

In this case only one function  $g_1 = \text{GPSE}(\cdot)$  is used to calculate the encodings. It is worth noting that random noise initialization is used in GPSE to help the model learn some of the more challenging PEs. To emulate this procedure, for all neighborhoods  $\mathcal{N} \in \mathcal{N}_C$ ,  $\mathcal{N}_C \subseteq \mathcal{N}_T$ , and their corresponding Hasse graphs  $\mathcal{J}_{\mathcal{N}}|_k = (\mathcal{C}_{\mathcal{N}}, \mathcal{E}_{\mathcal{N}}, \mathcal{F}_{\mathcal{N}})$ , the features  $F_{r,k} \in \mathcal{F}_{\mathcal{N}}$  are initialized as  $F_{r,k} \sim N(0, \mathbf{I}) \in \mathbb{R}^{20}$ .

### D.3 Learnable embedding functions

For the functions  $f_{r,k}$ ,  $\varepsilon_r$ , and  $\Theta_r$  HOPSE uses  $L$ -layer multilayer perceptrons (MLPs) with independent parameters. Each layer calculates the next embedding as:

$$\mathbf{h}_{r,k}^{(\ell)} = \sigma \left( \text{LayerNorm} \left( (\mathbf{h}_{r,k}^{(\ell-1)} \mathbf{W}_{r,k}^{(\ell)} + \mathbf{b}_{r,k}^{(\ell)}) + \mathbf{h}_{r,k}^{(\ell-1)} \right); \varepsilon = 10^{-6} \right), \quad (14)$$

where each  $\mathbf{W}_{r,k}^{(\ell)} \in \mathbb{R}^{D_r \times D_r}$  and  $\mathbf{b}_{r,k}^{(\ell)} \in \mathbb{R}^{D_r}$  are learned, an additional  $\mathbf{h}_{r,k}^{(\ell-1)}$  is added as a skip-connection,  $\text{LayerNorm}(\cdot; \varepsilon)$  normalizes to zero mean and unit variance with  $\varepsilon = 10^{-6}$  for numerical stability, and  $\sigma$  is the pointwise nonlinearity LeakyReLU. The final output  $\mathbf{h}_{r,k}^{(L)}$  yields the updated channel feature.

All MLPs share depth  $L$  but may vary in hidden-layer widths  $\{d_{r,\ell}\}$ . This unified design—with layer normalization before activation—ensures stable gradient flow and flexible expressivity across channels and ranks.

## E Complexity Analysis

To analyze the time complexity (in terms of FLOPs) of the HOPSE framework, distinguishing between two components is needed: (i) operations that can be precomputed once before training, and (ii) operations that must be performed during each training iteration.

**Preprocessing overhead.** For positional and structural encodings, although the functions  $g_k(\cdot)$  can, in principle, be any function—including trainable neural networks—the implementation is restricted to either graph-theoretic positional encodings or those generated by a pretrained GPSE model. This allows the tensors  $\mathbf{X}_{r,k}$  (as defined in equation 2) to be pre-computed before training begins.

This is helpful because certain positional encodings can be computationally expensive. For instance, using the eigenvectors of the graph Laplacian requires eigendecomposition of a matrix  $n \times n$ , which has a complexity of  $\mathcal{O}(n^3)$ . This makes such encodings impractical for large graphs if computed during training.

**Train time computation.** The trainable components of the HOPSE framework are the functions  $\varepsilon_r(\cdot)$ ,  $f_{r,k}(\cdot)$ , and  $\Theta_r(\cdot)$ , for all  $r = 1, \dots, R$  and  $k = 1, \dots, K$ . For these functions, HOPSE uses MLPs with  $L$  layers

An MLP with  $L$  layers applied to  $N$  elements with input and output dimensions  $D_{\text{in}}$  and  $D_{\text{out}}$  has a computational complexity of  $\mathcal{O}(ND_{\text{in}}D_{\text{out}})$ . For simplicity, let us consider fixed input and output dimensions for each rank. The complexity of generating the initial features  $\hat{\mathbf{Z}}_r$  in equation 4 is

$$\mathcal{O}(N_r D_r^2 L),$$

where  $N_r$  is the number of cells of rank  $r$ , and  $D_r$  is the feature dimension.

Next, the cost of computing  $\mathbf{X}_{r,k}$  for all  $K$  positional encodings (as in equation 3) is:

$$\mathcal{O}(N_r D_r^2 K L),$$

assuming that each function  $f_{r,k}$  preserves the feature dimensionality.

Assuming concatenation is used as the aggregation operation in equation 5, and that the output features have dimension  $D_r$ , the complexity of computing the final embeddings  $\mathbf{H}_r$  is:

$$\mathcal{O}(N_r D_r^2 (K + 1) L).$$

Combining all components, the total complexity for rank- $r$  cells is:

$$C_r = \mathcal{O}(N_r D_r^2 L + N_r D_r^2 K L + N_r D_r^2 (K + 1) L) = \mathcal{O}(N_r D_r^2 (K + 1) L).$$

The final complexity, assuming that all cells have the same input and hidden dimensions, is

$$C_{\text{HOPSE}} = \sum_{r=1}^R C_r.$$

This complexity scales linearly with the number of rank- $r$  cells and is independent of their connectivity. This is in sharp contrast with most higher-order neural architectures. For example, the Generalized Combinatorial Complex Neural Network (GCCN) analyzed in [39] has the following complexity:

$$C_{\text{GCCN}} = \sum_{\mathcal{N} \in \mathcal{N}_C} \mathcal{O}(\|\mathcal{N}\|_0 D^2 + \text{nrows}(\mathcal{N}) d_{r'} D + \text{nrows}(\mathcal{N})) + \sum_{r' \in [0, R']} n_{r'} n_{\mathcal{N}_{r'}} D,$$

where:

- $\mathcal{N}_C$  is the set of neighborhoods considered,
- $\mathcal{N}$  is a neighborhood from rank- $r$  to rank- $r'$  cells,
- $\|\mathcal{N}\|_0$  is the number of nonzero entries in  $\mathcal{N}$ ,
- $D$  is the feature dimension,
- $d_{r'}$  is the degree of rank- $r'$  cells (assumed constant),
- $n_{r'}$  is the number of rank- $r'$  cells,
- $n_{\mathcal{N}_{r'}}$  is the number of neighborhoods with target rank  $r'$ .

Unlike HOPSE, the GCCN complexity depends on the number of cells and the structure of their relationships.

**Summary.** This analysis shows that HOPSE achieves high expressive power (as demonstrated in Theorem 4.1) while maintaining a computational complexity that scales linearly with the number of cells. This is possible by offloading the structure-dependent computations to a one-time preprocessing step. The resulting efficiency, confirmed by the experimental results in Table 3, makes HOPSE well-suited for large-scale graph data.

## F Extended results

All experiments were performed on a Linux system with 256 CPU cores, 1TB of RAM, and 8 NVIDIA A30 GPUs, each with 24GB of GPU memory. The implementation code and reproduction materials will be released upon manuscript acceptance.

### F.1 Training and evaluation.

Five splits are generated for each dataset, with 50%/25%/25% of the data going to the training, validation, and test sets, respectively; the exception is ZINC, for which the predefined splits are used [27]. If available, this work considers the results reported in TopoBench for the baseline models. In the case of the HOPSE architecture and SANN baseline, the benchmarking of the corresponding architectures follows the predefined TopoBench suite.

Following the literature, different performance metrics are reported per dataset. Specifically, predictive accuracy is used for MUTAG, PROTEINS, NCI1, and NCI109. Mean absolute error (MAE) is used for ZINC. F1 score is used for MANTRA datasets. For each dataset, the mean and standard deviation of the chosen metric are computed across the five test sets.

### F.2 Hyperparameter search

The HOPSE architecture is optimized over eight variations in the neighborhood set. Each variation specifies a combination of neighborhoods. The considered neighborhood combinations are as follows:

- $\mathcal{A}_{0,1}$
- $\mathcal{A}_{0,1}, \mathcal{A}_{1,2}$
- $\mathcal{A}_{0,1}, \mathcal{A}_{1,2}, \mathcal{A}_{2,1}$
- $\mathcal{A}_{0,1}, \mathcal{I}_{0 \rightarrow 1}, \mathcal{I}_{1 \rightarrow 2}$
- $\mathcal{A}_{0,1}, \mathcal{I}_{1 \rightarrow 0}, \mathcal{I}_{2 \rightarrow 1}$
- $\mathcal{A}_{0,1}, \mathcal{I}_{0 \rightarrow 1}, \mathcal{I}_{1 \rightarrow 2}, \mathcal{I}_{1 \rightarrow 0}, \mathcal{I}_{2 \rightarrow 1}$

- $\mathcal{A}_{0,1}, \mathcal{A}_{1,2}, \mathcal{A}_{1,0}, \mathcal{A}_{2,1}, \mathcal{I}_{0 \rightarrow 1}, \mathcal{I}_{1 \rightarrow 2}, \mathcal{I}_{1 \rightarrow 0}, \mathcal{I}_{2 \rightarrow 1}$
- $\mathcal{A}_{0,1}, \mathcal{A}_{1,2}, \mathcal{A}_{0,2}, \mathcal{A}_{1,0}, \mathcal{A}_{2,1}, \mathcal{A}_{2,0}$

The first three configurations rely solely on adjacency-based neighborhoods. The following four integrate adjacency and incidence relations, while the final configuration includes jumps across ranks.

For both **HOPSE-M** and **HOPSE-G**, the set of neighborhood configurations described above is incorporated into the architecture search space, allowing the models to explore diverse neighborhoods.

**HOPSE-G** leverages the GPSE model to extract both positional and structural information. The evaluation is on four variants of the GPSE model, each pre-trained on a different dataset: ZINC, GEOM, MOLPCBA, and PCQM4MV2. These pre-trained models are treated as hyperparameters during the hyperparameter search. Overall, results show that GPSE models pre-trained on different datasets generalize well and consistently capture meaningful positional and structural features across all evaluated benchmarks, with no single pre-trained model consistently outperforming the others.

For the SANN model, the number of hops needed to define both positional and structural encodings was treated as an additional hyperparameter.

Finally, the search space over architecture parameters is restricted to hyperparameters that are common across all models: SANN, HOPSE, SCCNN, and SCN. A grid-search strategy is employed to identify the optimal parameters for each model-dataset combination. Specifically:

- Encoder hidden dimension: {32, 64, 128, 256}
- Encoder dropout: {0.25, 0.5}
- Number of backbone layers: {1, 2, 3, 4}
- Learning rate: {0.01, 0.001}
- Weight decay: {0, 0.0001}
- Batch size: {128, 256}

For SCN and SCCNN models, the considered readout types are *direct readout (DR)* and *signal down-propagation (SDP)* (refer to Telyatnikov et al. [42] for in-depth discussion on these options).

### F.3 Datasets

The datasets considered are five standard benchmarking datasets commonly used in the TDL literature, comprising four graph classification tasks and one graph regression task. The classification tasks use datasets from the TUDataset collection<sup>6</sup>—MUTAG, PROTEINS, NCI1, and NCI109 [35]. For regression, the ZINC dataset is used [27]. Following standard practice in the TDL literature [42], liftings are applied to transform these graph datasets into higher-order domains. Specifically, the cycle-based lifting was used for the cell domain, and the clique complex lifting for the simplicial domain.

Additionally, the MANTRA dataset comprises different triangulations of manifolds. A triangulation of a manifold  $\mathcal{M}$  is a pair  $(K, \iota)$  where  $K$  is a simplicial complex and  $\iota$  is a *homeomorphism* between  $\mathcal{M}$  and the geometric realization of  $K$ . Concretely, triangulations encode higher-order topological information that the underlying graph, or 0-skeleton, does not encode. Since some triangulations are non-homeomorphic but share an underlying graph, the ability to distinguish triangulations requires that the model can access the topological information to make the correct predictions. This dataset emphasizes benchmarking a model’s predictive ability on purely topological properties. Thus, it aims to assess how much the model encodes topological information beyond the base graph. In contrast to the MANTRA paper, this work does not enhance node features with any additional manually derived features but instead initializes features for all cells as ones.

Regarding  $\beta_0, \beta_1, \beta_2$ , following the Ballester et al. [2] work, in the case of predicting Betti numbers, this work focuses on training a single model as a multivariate regression task to report corresponding results for each Betti number. The choice of using F1 over AUROC is based on class imbalances of the Betti numbers  $\beta_0, \beta_1, \beta_2$  and of the predicted properties name (NAME) and orientability ORIENT.

---

<sup>6</sup>Although these datasets are relatively dated, they remain widely adopted as a benchmarking suite in TDL research, offering consistent baselines for comparative evaluation

#### F.4 Runtime per epoch

In these experiments, the runtime per epoch is shown for each dataset. Table 4 shows the average runtime per epoch on the benchmarked datasets. Our method has the lowest runtime per epoch across all datasets among HOMP methods. These results validate the theoretical findings presented. In addition, **HOPSE-G** is faster than **HOPSE-M** in all benchmarks except NCI109. This aligns with complexity and scales linearly with the number  $K$  of positional encodings considered.

Compared to graph message passing methods, such as GCN, GAT, and GIN, the HOPSE framework performs competitively on smaller datasets such as MUTAG, PROTEINS, NCI1, and NCI109. On larger datasets, it speeds up up to 4x in ZINC and closer to 2x in MANTRA.

Table 4: Runtime per epoch in seconds. Results are shown as mean and standard deviation. The best result per domain and per model is in **bold** and results within one standard deviation of the lowest per domain are highlighted in blue. The **HOPSE** framework is *more efficient* than all other HOMP-based methods across all datasets. In the larger datasets such as ZINC and MANTRA, it is *more efficient* than traditional message passing over graphs. The variation between the *simplicial* and *cell* domain for both models is relatively low

Model	Graph Tasks					Topological Tasks		
	MUTAG	PROTEINS	NCI1	NCI109	ZINC	NAME	ORIENT	$(\beta_0, \beta_1, \beta_2)$
Graph	GCN	<b>0.03 ± 0.00</b>	<b>0.05 ± 0.00</b>	<b>0.26 ± 0.01</b>	<b>0.27 ± 0.02</b>	1.24 ± 0.01	<b>6.24 ± 0.11</b>	6.24 ± 0.10
	GAT	0.04 ± 0.00	0.07 ± 0.00	0.34 ± 0.02	0.33 ± 0.02	1.24 ± 0.01	6.38 ± 0.14	<b>6.16 ± 0.12</b>
	GIN	<b>0.03 ± 0.00</b>	0.06 ± 0.00	0.27 ± 0.02	<b>0.27 ± 0.02</b>	<b>1.19 ± 0.00</b>	6.37 ± 0.12	6.18 ± 0.06
Simplicial	SCN	0.09 ± 0.00	0.42 ± 0.01	1.60 ± 0.03	1.59 ± 0.02	6.93 ± 0.09	6.83 ± 0.08	7.35 ± 0.38
	SCCNN	0.09 ± 0.00	0.43 ± 0.01	1.65 ± 0.02	1.66 ± 0.03	10.40 ± 0.06	8.47 ± 0.63	8.25 ± 0.12
	SaNN	0.03 ± 0.00	0.18 ± 0.00	0.64 ± 0.02	0.65 ± 0.02	0.63 ± 0.03	7.21 ± 0.08	7.77 ± 0.15
	GCCN	0.04 ± 0.00	3.06 ± 0.02	0.43 ± 0.02	0.39 ± 0.02	-	6.79 ± 0.24	6.13 ± 0.09
	HOPSE-M	<b>0.02 ± 0.00</b>	0.12 ± 0.00	0.32 ± 0.00	0.47 ± 0.03	0.35 ± 0.01	5.13 ± 0.14	5.60 ± 0.55
	HOPSE-G	<b>0.02 ± 0.00</b>	<b>0.10 ± 0.02</b>	<b>0.31 ± 0.00</b>	<b>0.37 ± 0.02</b>	<b>0.28 ± 0.01</b>	<b>4.48 ± 0.14</b>	<b>4.23 ± 0.12</b>
Cell	CCCN	0.11 ± 0.00	0.32 ± 0.01	1.33 ± 0.02	1.33 ± 0.02	6.14 ± 0.04	-	-
	CWN	0.10 ± 0.00	0.37 ± 0.02	1.38 ± 0.03	1.37 ± 0.01	5.86 ± 0.05	-	-
	HOPSE-M	<b>0.02 ± 0.00</b>	0.13 ± 0.01	<b>0.34 ± 0.00</b>	<b>0.33 ± 0.01</b>	0.47 ± 0.02	-	-
	HOPSE-G	<b>0.02 ± 0.00</b>	<b>0.09 ± 0.00</b>	0.40 ± 0.02	0.37 ± 0.00	<b>0.32 ± 0.01</b>	-	-

#### F.5 Ablation on neighborhood set $\mathcal{N}_C$

To gain more insight into how the choice of neighborhoods  $\mathcal{N}_C$  impacts the performance of the HOPSE framework, this section shows an ablation over the considered sets of neighborhoods. The neighborhood sets listed in the tables are defined in Table 5. Each configuration differs in the number and type of neighborhoods considered, directly influencing computational complexity and model expressivity. Specifically, the *Adj* family explores adjacency-based neighborhoods of increasing order: *Adj-1* uses a single neighborhood, while *Adj-2* and *Adj-3* consider two and three neighborhoods, respectively. The *Inc* configurations mix the base adjacency ( $\mathcal{A}_{0,1}$ ) and incidence, with *Inc-1* and *Inc-2* using three neighborhoods, and *Inc-3* extending to five. The *Mix* configurations, *Mix-1* and *Mix-2*, are the biggest, combining a total of eight and six neighborhoods, respectively. *Mix-1* uses all previous adjacencies and incidences combined while *Mix-2* includes more complex neighborhoods. One of such is  $\mathcal{A}_{0,2}$ , which means the adjacencies of 0-cells with 2-cells *through* 1-cells. Effectively, this means that the structure of neighborhoods between non-adjacent ranks (i.e., a difference of 1 in the rank number) is considered. As will be seen later in the section, considering these non-standard neighborhoods does account for a difference in performance for the more complex benchmarks.

Table 5: Taxonomy of neighborhood combinations

Group	Neighborhood Combination
<i>Adj-1</i>	$\mathcal{A}_{0,1}$
<i>Adj-2</i>	$\mathcal{A}_{0,1}, \mathcal{A}_{1,2}$
<i>Adj-3</i>	$\mathcal{A}_{0,1}, \mathcal{A}_{1,2}, \mathcal{A}_{2,1}$
<i>Inc-1</i>	$\mathcal{A}_{0,1}, \mathcal{I}_{0 \rightarrow 1}, \mathcal{I}_{1 \rightarrow 2}$
<i>Inc-2</i>	$\mathcal{A}_{0,1}, \mathcal{I}_{1 \rightarrow 0}, \mathcal{I}_{2 \rightarrow 1}$
<i>Inc-3</i>	$\mathcal{A}_{0,1}, \mathcal{I}_{0 \rightarrow 1}, \mathcal{I}_{1 \rightarrow 2}, \mathcal{I}_{1 \rightarrow 0}, \mathcal{I}_{2 \rightarrow 1}$
<i>Mix-1</i>	$\mathcal{A}_{0,1}, \mathcal{A}_{1,2}, \mathcal{A}_{1,0}, \mathcal{A}_{2,1}, \mathcal{I}_{0 \rightarrow 1}, \mathcal{I}_{1 \rightarrow 2}, \mathcal{I}_{0 \rightarrow 1}, \mathcal{I}_{2 \rightarrow 1}$
<i>Mix-2</i>	$\mathcal{A}_{0,1}, \mathcal{A}_{1,2}, \mathcal{A}_{0,2}, \mathcal{A}_{1,0}, \mathcal{A}_{2,1}, \mathcal{A}_{2,0}$

Table 6: Performance per neighborhood on *simplicial*. Results are shown as mean  $\pm$  standard deviation. The best result per neighborhood is in **bold** and results within one standard deviation of the best per neighborhood are highlighted in blue. The performance differences between neighborhood configurations are minimal, with most results falling within one standard deviation of each other. As datasets grow bigger and more complex, such as ZINC and the MANTRA benchmarks, the neighborhood choice starts to matter. The results show that for simplicial models, the most informative neighborhoods for ZINC are the extended groups of adjacencies *Adj-2* and *Adj-3*. However, for the MANTRA tasks, the most important neighborhood is *Mix-2*

Nbhd	Graph Tasks					Topological Tasks			
	MUTAG ( $\uparrow$ )	PROTEINS ( $\uparrow$ )	NCII ( $\uparrow$ )	NCII09 ( $\uparrow$ )	ZINC ( $\downarrow$ )	NAME ( $\uparrow$ )	ORIENT ( $\uparrow$ )	$\beta_1$ ( $\uparrow$ )	$\beta_2$ ( $\uparrow$ )
<b>HOPSE-M</b>	<b>Adj-1</b> <b>86.38 <math>\pm</math> 6.31</b>	74.70 $\pm$ 4.04	<b>77.35 <math>\pm</math> 0.81</b>	75.41 $\pm$ 1.17	0.40 $\pm$ 0.01	79.58 $\pm$ 2.88	60.93 $\pm$ 3.03	88.35 $\pm$ 0.09	28.25 $\pm$ 2.71
	<b>Adj-2</b> 85.53 $\pm$ 7.12	73.19 $\pm$ 3.32	76.26 $\pm$ 1.59	75.59 $\pm$ 0.41	<b>0.39 <math>\pm</math> 0.02</b>	80.35 $\pm$ 3.96	74.63 $\pm$ 1.77	89.97 $\pm$ 0.18	64.06 $\pm$ 2.27
	<b>Adj-3</b> 85.96 $\pm$ 5.75	<b>75.13 <math>\pm</math> 3.66</b>	76.44 $\pm$ 1.44	75.22 $\pm$ 2.06	<b>0.39 <math>\pm</math> 0.02</b>	84.72 $\pm$ 1.23	78.19 $\pm$ 2.70	90.13 $\pm$ 0.49	70.10 $\pm$ 1.86
<i>Inc-1</i>	85.11 $\pm$ 6.20	73.98 $\pm$ 2.97	76.40 $\pm$ 0.99	76.09 $\pm$ 1.50	0.40 $\pm$ 0.01	84.01 $\pm$ 6.84	65.10 $\pm$ 9.66	<b>90.06 <math>\pm</math> 0.09</b>	65.02 $\pm$ 1.58
	<i>Inc-2</i> 84.26 $\pm$ 6.13	73.69 $\pm$ 2.76	76.40 $\pm$ 1.45	75.39 $\pm$ 1.13	0.42 $\pm$ 0.05	80.67 $\pm$ 2.88	69.51 $\pm$ 6.86	89.51 $\pm$ 0.94	64.28 $\pm$ 3.08
	<i>Inc-3</i> 85.11 $\pm$ 5.83	73.55 $\pm$ 3.38	76.56 $\pm$ 1.40	<b>76.34 <math>\pm</math> 1.40</b>	0.42 $\pm$ 0.02	82.56 $\pm$ 4.15	77.35 $\pm$ 2.12	89.89 $\pm$ 0.13	63.12 $\pm$ 1.68
<i>Mix-1</i>	84.26 $\pm$ 5.12	73.69 $\pm$ 3.21	76.44 $\pm$ 1.62	<b>75.57 <math>\pm</math> 1.09</b>	0.40 $\pm$ 0.01	90.37 $\pm$ 1.29	72.64 $\pm$ 7.53	90.21 $\pm$ 0.18	67.14 $\pm$ 2.18
	<i>Mix-2</i> 83.83 $\pm$ 6.49	73.41 $\pm$ 2.95	75.14 $\pm$ 1.59	74.87 $\pm$ 0.94	0.41 $\pm$ 0.02	<b>91.50 <math>\pm</math> 1.45</b>	<b>80.68 <math>\pm</math> 1.72</b>	<b>90.26 <math>\pm</math> 0.55</b>	<b>71.69 <math>\pm</math> 1.50</b>
	<b>HOPSE-G</b>	<b>Adj-1</b> 82.98 $\pm$ 7.22	74.05 $\pm$ 2.17	<b>77.18 <math>\pm</math> 1.45</b>	76.21 $\pm$ 0.65	0.44 $\pm$ 0.01	80.43 $\pm$ 1.03	60.92 $\pm$ 1.18	88.18 $\pm$ 0.03
		<b>Adj-2</b> <b>85.53 <math>\pm</math> 2.77</b>	74.05 $\pm$ 3.08	77.51 $\pm$ 1.15	74.91 $\pm$ 1.17	<b>0.43 <math>\pm</math> 0.00</b>	80.19 $\pm$ 1.13	61.88 $\pm$ 0.83	88.13 $\pm$ 0.02
		<b>Adj-3</b> 85.11 $\pm$ 3.36	73.26 $\pm$ 4.20	77.32 $\pm$ 1.19	74.79 $\pm$ 0.91	<b>0.43 <math>\pm</math> 0.01</b>	79.11 $\pm$ 1.53	61.86 $\pm$ 1.10	88.11 $\pm$ 0.02
<i>Inc-1</i>	84.68 $\pm$ 3.50	73.19 $\pm$ 3.52	<b>77.70 <math>\pm</math> 1.40</b>	<b>76.36 <math>\pm</math> 1.75</b>	0.44 $\pm$ 0.00	80.70 $\pm$ 0.80	<b>62.17 <math>\pm</math> 0.98</b>	87.31 $\pm$ 1.17	20.47 $\pm$ 3.22
	<i>Inc-2</i> 82.13 $\pm$ 5.75	<b>76.27 <math>\pm</math> 2.10</b>	75.66 $\pm$ 1.52	74.17 $\pm$ 1.99	0.45 $\pm$ 0.02	78.92 $\pm$ 1.25	59.57 $\pm$ 1.56	88.08 $\pm$ 0.08	20.28 $\pm$ 3.48
	<i>Inc-3</i> 77.87 $\pm$ 4.90	75.48 $\pm$ 3.15	76.15 $\pm$ 1.77	<b>75.14 <math>\pm</math> 0.75</b>	0.44 $\pm$ 0.01	78.78 $\pm$ 0.74	60.35 $\pm$ 1.05	88.12 $\pm$ 0.04	18.82 $\pm$ 3.54
<i>Mix-1</i>	79.15 $\pm$ 7.88	75.70 $\pm$ 3.24	76.50 $\pm$ 1.09	75.35 $\pm$ 0.97	0.45 $\pm$ 0.01	79.76 $\pm$ 0.51	60.33 $\pm$ 1.60	88.07 $\pm$ 0.09	23.48 $\pm$ 3.44
	<i>Mix-2</i> 83.40 $\pm$ 8.56	74.05 $\pm$ 3.39	77.02 $\pm$ 0.92	74.75 $\pm$ 1.47	0.46 $\pm$ 0.01	<b>81.75 <math>\pm</math> 1.26</b>	61.32 $\pm$ 2.67	<b>88.28 <math>\pm</math> 0.08</b>	<b>35.37 <math>\pm</math> 2.25</b>

### F.5.1 Analysis of performance across neighborhoods

**Analysis of performance for different domains.** The results in Table 6 and Table 7 demonstrate insightful patterns in how neighborhood selection impacts performance depending on domain type and dataset complexity. Comparing performance between **HOPSE-M** and **HOPSE-G** variants across different neighborhood configurations further suggests that the pre-training strategy employed in GPSE provides rich neighborhood information, particularly for the molecular datasets, as the GPSE encoder has been pre-trained on molecular data. This is most evident in the cell domain results for ZINC, where **HOPSE-G** with *Mix-2* achieves a 16% improvement compared to the best **HOPSE-M** configuration.

**Efficacy of neighborhoods by domain.** One important observation is how neighborhood efficacy varies between the simplicial and cell domains. While in the simplicial domain, adding mixed neighborhoods occasionally leads to performance degradation for some datasets (e.g., PROTEINS where *Inc-1* outperforms *Mix* configurations for **HOPSE-M**), in the cell domain, more comprehensive neighborhood sets either improve or do not significantly impact performance. This domain-dependent behavior suggests that the optimal neighborhood configuration should be ideally selected based on task complexity and the topological representation chosen for the data; however, choosing comprehensive neighborhood sets on average allows for achieving good performance while not

Table 7: Performance per neighborhood on *cell*. Results are shown as mean  $\pm$  standard deviation. The best result per domain and model is in **bold** and results within one standard deviation of the lowest per domain are highlighted in blue. In smaller and simpler datasets such as MUTAG, PROTEINS, NCI1, and NCI109, the best neighborhoods are not always the most encompassing, but they perform closely to others. However, on a more complex dataset such as ZINC there is a significant difference between simpler neighborhoods like the *Adj-1/3* and *Mix-2*, particularly in the case of **HOPSE-G**.

		Graph Tasks				
Nbhd		MUTAG ( $\uparrow$ )	PROTEINS ( $\uparrow$ )	NCI1 ( $\uparrow$ )	NCI109 ( $\uparrow$ )	ZINC ( $\downarrow$ )
<b>HOPSE-M</b>	<i>Adj-1</i>	<b><math>88.09 \pm 5.55</math></b>	$75.77 \pm 2.67$	$76.85 \pm 0.83$	$76.34 \pm 1.02$	$0.29 \pm 0.01$
	<i>Adj-2</i>	$82.13 \pm 4.15$	$74.55 \pm 2.65$	<b><math>78.09 \pm 1.44</math></b>	<b><math>77.27 \pm 1.01</math></b>	$0.27 \pm 0.01$
	<i>Adj-3</i>	$85.53 \pm 3.50$	$75.27 \pm 2.19$	$77.57 \pm 1.48$	$75.37 \pm 0.79$	$0.28 \pm 0.01$
	<i>Inc-1</i>	$86.81 \pm 4.61$	<b><math>76.99 \pm 2.63</math></b>	$77.32 \pm 1.62$	$75.70 \pm 1.36$	$0.27 \pm 0.02$
	<i>Inc-2</i>	$83.40 \pm 3.81$	$75.56 \pm 2.26$	$75.89 \pm 2.14$	$75.43 \pm 1.98$	$0.29 \pm 0.02$
	<i>Inc-3</i>	$82.98 \pm 3.36$	$74.70 \pm 3.05$	$77.14 \pm 0.46$	$74.46 \pm 1.52$	<b><math>0.25 \pm 0.01</math></b>
	<i>Mix-1</i>	$81.28 \pm 5.90$	$75.13 \pm 3.09$	$77.26 \pm 1.70$	$76.13 \pm 1.38$	<b><math>0.25 \pm 0.01</math></b>
	<i>Mix-2</i>	$84.26 \pm 6.13$	$72.62 \pm 2.55$	$76.69 \pm 1.25$	$76.57 \pm 1.55$	$0.26 \pm 0.01$
	<i>Adj-1</i>	$82.13 \pm 7.76$	$76.27 \pm 2.70$	$78.31 \pm 0.84$	$77.48 \pm 0.99$	$0.26 \pm 0.00$
<b>HOPSE-G</b>	<i>Adj-2</i>	$87.66 \pm 6.96$	<b><math>76.42 \pm 2.19</math></b>	$78.83 \pm 1.40$	$77.48 \pm 0.64$	$0.24 \pm 0.00$
	<i>Adj-3</i>	<b><math>88.09 \pm 1.90</math></b>	$75.91 \pm 1.89$	$78.35 \pm 1.11$	$76.94 \pm 1.46$	$0.23 \pm 0.00$
	<i>Inc-1</i>	$85.11 \pm 6.56$	$74.62 \pm 3.99$	$77.57 \pm 1.67$	$76.81 \pm 1.23$	$0.25 \pm 0.01$
	<i>Inc-2</i>	$82.55 \pm 8.82$	$74.91 \pm 2.11$	$78.15 \pm 0.75$	$76.40 \pm 1.86$	$0.27 \pm 0.01$
	<i>Inc-3</i>	$84.68 \pm 7.88$	$74.12 \pm 3.39$	$76.81 \pm 0.59$	$75.26 \pm 1.16$	$0.26 \pm 0.00$
	<i>Mix-1</i>	<b><math>88.09 \pm 3.23</math></b>	$76.20 \pm 2.62$	$79.03 \pm 0.73$	$76.88 \pm 0.95$	$0.23 \pm 0.00$
	<i>Mix-2</i>	$85.11 \pm 6.02$	$75.63 \pm 2.35$	<b><math>79.07 \pm 0.65</math></b>	<b><math>77.81 \pm 1.26</math></b>	<b><math>0.21 \pm 0.01</math></b>

harming the computational cost (see Appendix F.5.2 for details on computational analysis). These findings demonstrate that the choice of neighborhood configuration represents a critical design decision in topological learning frameworks. While simpler configurations may suffice for some graph benchmarks, an effective strategy is to consider a greater neighbourhood set  $\mathcal{N}_C$  to capture the full expressive power of topological structures. It is especially evident on complex tasks, topological benchmarking datasets (MANTRA), and relatively large datasets like ZINC.

### F.5.2 Analysis of time efficiency across neighborhoods

This section presents the effects of the choice of  $\mathcal{N}_C$  on the total runtime and per-epoch performance of the HOPSE framework. The results in Table 8 and Table 9 report the per-epoch runtime for each neighborhood configuration across both the simplicial and cell domains, under the **HOPSE-M** and **HOPSE-G** models, respectively. While Table 10 and Table 11 present the total runtime to convergence for eight different neighbourhoods for simplicial and cell domains, and **HOPSE-M** and **HOPSE-G** correspondingly.

**Runtime per epoch per neighborhood.** As expected Table 8 and Table 9 show that the runtime per epoch increases as the number of neighborhoods in  $\mathcal{N}_C$  increases. This aligns with the complexity analysis presented in Appendix E. Still, the relative increase in computational time is at most 80%, which is acceptable when considering how many more higher-order relations are being considered.

The efficiency-expressivity trade-off revealed in these results has important implications for the practical deployment. While intuition might suggest that more complex neighborhood configurations would always incur substantial computational penalties, our findings demonstrate that this is not necessarily true.

Despite incorporating significantly more structural information, complex neighborhood configurations like *Mix-1* and *Mix-2* introduce only a modest increase in per-epoch runtime, typically less than 2 $\times$  compared to the simplest configurations. This makes them viable options even in computationally constrained environments.

**Total runtime per neighborhood.** The total runtime required to reach convergence, presented in Table 10 and Table 11, reveals more nuanced patterns. Unlike per-epoch runtime, total runtime

Table 8: Runtime per epoch per neighborhood on *simplicial*. Results are shown as mean  $\pm$  standard deviation. The best result per domain and model is in **bold** and results within one standard deviation of the lowest per domain are highlighted in blue. Simpler configurations such as *Adj-1* consistently yield the lowest runtime across domains, particularly for **HOPSE-M**, where *Adj-1* achieves the fastest epoch times in 5 out of 8 datasets,

		Graph Tasks				Topological Tasks				
		Nbhd	MUTAG	PROTEINS	NCI1	NCI109	ZINC	NAME	ORIENT	$(\beta_0, \beta_1, \beta_2)$
<b>HOPSE-M</b>	<i>Adj-1</i>	<b>0.02 <math>\pm</math> 0.00</b>	0.12 $\pm$ 0.01	<b>0.32 <math>\pm</math> 0.00</b>	<b>0.32 <math>\pm</math> 0.00</b>	<b>0.30 <math>\pm</math> 0.01</b>	<b>4.12 <math>\pm</math> 0.08</b>	4.41 $\pm$ 0.11	<b>4.48 <math>\pm</math> 0.16</b>	
	<i>Adj-2</i>	0.03 $\pm$ 0.01	<b>0.12 <math>\pm</math> 0.00</b>	0.36 $\pm$ 0.01	0.36 $\pm$ 0.00	0.35 $\pm$ 0.01	4.37 $\pm$ 0.13	<b>4.15 <math>\pm</math> 0.09</b>	4.54 $\pm$ 0.21	
	<i>Adj-3</i>	0.02 $\pm$ 0.00	0.12 $\pm$ 0.01	0.37 $\pm$ 0.00	0.39 $\pm$ 0.00	0.37 $\pm$ 0.01	4.42 $\pm$ 0.11	4.41 $\pm$ 0.22	4.91 $\pm$ 0.07	
	<i>Inc-1</i>	0.03 $\pm$ 0.00	0.14 $\pm$ 0.01	0.44 $\pm$ 0.01	0.40 $\pm$ 0.01	0.40 $\pm$ 0.01	6.28 $\pm$ 1.34	5.14 $\pm$ 0.24	5.41 $\pm$ 0.17	
	<i>Inc-2</i>	0.03 $\pm$ 0.01	0.12 $\pm$ 0.01	0.36 $\pm$ 0.00	0.39 $\pm$ 0.00	0.34 $\pm$ 0.01	4.41 $\pm$ 0.05	4.29 $\pm$ 0.06	4.87 $\pm$ 0.12	
	<i>Inc-3</i>	0.02 $\pm$ 0.00	0.16 $\pm$ 0.00	0.46 $\pm$ 0.01	0.47 $\pm$ 0.03	0.42 $\pm$ 0.01	5.89 $\pm$ 0.31	5.71 $\pm$ 0.23	5.70 $\pm$ 0.23	
<b>HOPSE-G</b>	<i>Mix-1</i>	0.03 $\pm$ 0.00	0.17 $\pm$ 0.01	0.51 $\pm$ 0.00	0.51 $\pm$ 0.02	0.48 $\pm$ 0.01	6.00 $\pm$ 0.29	6.25 $\pm$ 0.31	6.51 $\pm$ 0.23	
	<i>Mix-2</i>	0.02 $\pm$ 0.00	0.15 $\pm$ 0.00	0.45 $\pm$ 0.01	0.44 $\pm$ 0.00	0.40 $\pm$ 0.01	5.13 $\pm$ 0.14	5.60 $\pm$ 0.55	5.54 $\pm$ 0.05	
	<i>Adj-1</i>	<b>0.02 <math>\pm</math> 0.00</b>	<b>0.10 <math>\pm</math> 0.01</b>	<b>0.28 <math>\pm</math> 0.01</b>	<b>0.28 <math>\pm</math> 0.00</b>	<b>0.26 <math>\pm</math> 0.02</b>	<b>3.19 <math>\pm</math> 0.09</b>	<b>3.18 <math>\pm</math> 0.12</b>	<b>3.55 <math>\pm</math> 0.12</b>	
	<i>Adj-2</i>	0.02 $\pm$ 0.00	0.12 $\pm$ 0.01	0.30 $\pm$ 0.00	0.31 $\pm$ 0.01	0.28 $\pm$ 0.01	3.53 $\pm$ 0.12	3.41 $\pm$ 0.10	3.67 $\pm$ 0.12	
	<i>Adj-3</i>	0.02 $\pm$ 0.00	0.11 $\pm$ 0.00	0.33 $\pm$ 0.02	0.34 $\pm$ 0.01	0.29 $\pm$ 0.02	3.79 $\pm$ 0.14	3.84 $\pm$ 0.14	3.98 $\pm$ 0.07	
	<i>Inc-1</i>	0.02 $\pm$ 0.00	0.13 $\pm$ 0.01	0.38 $\pm$ 0.01	0.37 $\pm$ 0.02	0.34 $\pm$ 0.01	4.44 $\pm$ 0.14	4.23 $\pm$ 0.12	4.64 $\pm$ 0.08	
<b>HOPSE-G</b>	<i>Inc-2</i>	0.02 $\pm$ 0.00	<b>0.10 <math>\pm</math> 0.00</b>	<b>0.31 <math>\pm</math> 0.00</b>	<b>0.31 <math>\pm</math> 0.00</b>	<b>0.28 <math>\pm</math> 0.01</b>	<b>3.74 <math>\pm</math> 0.17</b>	<b>3.66 <math>\pm</math> 0.10</b>	<b>3.78 <math>\pm</math> 0.06</b>	
	<i>Inc-3</i>	0.02 $\pm$ 0.00	0.13 $\pm$ 0.00	0.41 $\pm$ 0.00	0.40 $\pm$ 0.01	0.38 $\pm$ 0.03	5.17 $\pm$ 0.40	4.75 $\pm$ 0.23	5.13 $\pm$ 0.06	
	<i>Mix-1</i>	0.02 $\pm$ 0.00	0.16 $\pm$ 0.01	0.46 $\pm$ 0.02	0.46 $\pm$ 0.01	0.44 $\pm$ 0.01	5.50 $\pm$ 0.24	5.74 $\pm$ 0.22	5.84 $\pm$ 0.38	
	<i>Mix-2</i>	0.02 $\pm$ 0.00	0.13 $\pm$ 0.01	0.38 $\pm$ 0.00	0.38 $\pm$ 0.01	0.36 $\pm$ 0.02	4.48 $\pm$ 0.14	4.55 $\pm$ 0.19	4.84 $\pm$ 0.11	

encapsulates both computational cost per epoch and the number of epochs to convergence, which are indirectly influenced by the expressiveness of the neighborhood structure. Interestingly, richer neighborhood configurations, despite their potentially higher per-epoch cost, often lead to a similar relative increase in time needed as the per-epoch case. This means that the number of epochs needed for convergence stays relatively constant.

**Optimal configurations.** For simpler graph classification tasks, simpler neighborhood configurations may offer the best efficiency. In contrast, more expressive neighborhood sets often provide better efficiency-accuracy trade-offs for complex topological tasks and larger datasets. These findings demonstrate that the choice of neighborhood configuration represents a critical design decision not just for model accuracy, but also for computational efficiency. The provided analysis presents a principled approach to neighborhood selection based on task requirements and domain characteristics, establishing an essential foundation for applying TDL to new fields.

### F.5.3 Preprocessing time per neighborhood

**Preprocessing time analysis** The computational costs of extracting positional and structural encodings are summarized in Tables 12 and 13. While preprocessing times scale with the complexity of the selected neighborhoods and not only with the number of cells, two points need to be emphasized:

1. **One time preprocessing:** Encodings are precomputed *once* per dataset, enabling efficient experimentation. For instance, preprocessing all neighborhoods for ZINC in the cell domain takes 25–30 minutes (e.g., 1,776 seconds for *Mix-1* in **HOPSE-G**), but this cost is amortized over all subsequent training runs. The practitioners can freely test configurations like *Adj-3* or *Inc-2* without recomputing features, streamlining hyperparameter optimization. Finally, the precomputed encodings can be shared, reducing redundant computation.
2. **Parallel computation:** The reported precomputation time results can be easily optimized by parallel precomputation.

Table 9: Runtime per epoch per neighborhood on *cell*. Results are shown as mean  $\pm$  standard deviation. The best result per domain and model is in **bold** and results within one standard deviation of the lowest per domain are highlighted in blue.

Graph Tasks						
Nbhd		MUTAG	PROTEINS	NCI1	NCI109	ZINC
HOPSE-M	<i>Adj-1</i>	<b>0.02 <math>\pm</math> 0.00</b>	0.11 $\pm$ 0.00	<b>0.31 <math>\pm</math> 0.01</b>	<b>0.32 <math>\pm</math> 0.01</b>	0.30 $\pm$ 0.01
	<i>Adj-2</i>	0.02 $\pm$ 0.00	0.11 $\pm$ 0.00	0.34 $\pm$ 0.00	0.33 $\pm$ 0.00	<b>0.30 <math>\pm</math> 0.01</b>
	<i>Adj-3</i>	0.02 $\pm$ 0.00	<b>0.11 <math>\pm</math> 0.00</b>	0.35 $\pm$ 0.00	0.34 $\pm$ 0.00	0.32 $\pm$ 0.01
	<i>Inc-1</i>	0.02 $\pm$ 0.00	0.13 $\pm$ 0.01	0.40 $\pm$ 0.01	0.40 $\pm$ 0.02	0.37 $\pm$ 0.02
	<i>Inc-2</i>	0.02 $\pm$ 0.00	<b>0.12 <math>\pm</math> 0.00</b>	0.35 $\pm$ 0.01	0.34 $\pm$ 0.01	0.32 $\pm$ 0.01
	<i>Inc-3</i>	0.03 $\pm$ 0.01	0.15 $\pm$ 0.00	0.42 $\pm$ 0.01	0.43 $\pm$ 0.01	0.41 $\pm$ 0.01
HOPSE-G	<i>Mix-1</i>	0.03 $\pm$ 0.00	0.16 $\pm$ 0.01	0.50 $\pm$ 0.01	0.54 $\pm$ 0.01	0.47 $\pm$ 0.02
	<i>Mix-2</i>	0.02 $\pm$ 0.00	0.13 $\pm$ 0.00	0.47 $\pm$ 0.02	0.46 $\pm$ 0.00	0.39 $\pm$ 0.01
	<i>Adj-1</i>	<b>0.02 <math>\pm</math> 0.00</b>	0.09 $\pm$ 0.01	<b>0.25 <math>\pm</math> 0.01</b>	<b>0.26 <math>\pm</math> 0.01</b>	<b>0.24 <math>\pm</math> 0.00</b>
	<i>Adj-2</i>	0.02 $\pm$ 0.00	<b>0.09 <math>\pm</math> 0.00</b>	0.29 $\pm$ 0.01	0.27 $\pm$ 0.01	0.26 $\pm$ 0.01
	<i>Adj-3</i>	0.02 $\pm$ 0.00	0.10 $\pm$ 0.00	0.32 $\pm$ 0.01	0.32 $\pm$ 0.02	0.27 $\pm$ 0.01
	<i>Inc-1</i>	0.02 $\pm$ 0.00	0.11 $\pm$ 0.00	0.37 $\pm$ 0.01	0.34 $\pm$ 0.00	0.33 $\pm$ 0.00
HOPSE-G	<i>Inc-2</i>	0.02 $\pm$ 0.00	<b>0.09 <math>\pm</math> 0.00</b>	0.32 $\pm$ 0.01	0.30 $\pm$ 0.05	0.28 $\pm$ 0.02
	<i>Inc-3</i>	0.02 $\pm$ 0.00	0.14 $\pm$ 0.01	0.40 $\pm$ 0.00	0.37 $\pm$ 0.00	0.36 $\pm$ 0.02
	<i>Mix-1</i>	0.03 $\pm$ 0.00	0.14 $\pm$ 0.00	0.44 $\pm$ 0.01	0.45 $\pm$ 0.00	0.42 $\pm$ 0.00
	<i>Mix-2</i>	0.02 $\pm$ 0.00	0.14 $\pm$ 0.00	0.40 $\pm$ 0.02	0.37 $\pm$ 0.01	0.32 $\pm$ 0.01

Table 10: Total runtime per neighborhood on *simplicial*. Results are shown as mean  $\pm$  standard deviation. The best result per domain and model is in **bold** and results within one standard deviation of the lowest per domain are highlighted in blue. HOPSE configurations, especially with mixed neighborhood sets, provide an excellent balance between efficiency and expressiveness.

		Graph Tasks					Topological Tasks		
Nbhd		MUTAG	PROTEINS	NCI1	NCI109	ZINC	NAME	ORIENT	$(\beta_0, \beta_1, \beta_2)$
HOPSE-M	<i>Adj-1</i>	<b>6.76 <math>\pm</math> 1.38</b>	44.60 $\pm$ 17.17	164.10 $\pm$ 79.48	<b>125.46 <math>\pm</math> 19.54</b>	1238.09 $\pm$ 378.91	<b>2652.62 <math>\pm</math> 67.51</b>	3028.14 $\pm$ 41.05	5327.90 $\pm$ 1334.91
	<i>Adj-2</i>	8.66 $\pm$ 0.51	<b>31.26 <math>\pm</math> 15.10</b>	165.10 $\pm$ 31.84	131.47 $\pm$ 24.84	1512.34 $\pm$ 310.43	3036.30 $\pm$ 1105.71	<b>2535.98 <math>\pm</math> 45.80</b>	<b>4053.39 <math>\pm</math> 718.36</b>
	<i>Adj-3</i>	6.87 $\pm$ 1.54	38.41 $\pm$ 8.07	175.02 $\pm$ 49.19	146.19 $\pm$ 27.88	1061.11 $\pm$ 404.64	2734.33 $\pm$ 156.56	2689.60 $\pm$ 38.86	4266.24 $\pm$ 651.78
	<i>Inc-1</i>	8.52 $\pm$ 1.47	41.92 $\pm$ 5.67	194.90 $\pm$ 64.73	206.44 $\pm$ 16.44	1183.26 $\pm$ 135.82	4351.87 $\pm$ 1203.66	3342.21 $\pm$ 88.20	5172.86 $\pm$ 1084.20
	<i>Inc-2</i>	10.37 $\pm$ 2.21	40.03 $\pm$ 20.40	<b>161.40 <math>\pm</math> 39.23</b>	180.17 $\pm$ 22.35	<b>895.12 <math>\pm</math> 295.76</b>	2704.44 $\pm$ 23.84	2998.32 $\pm$ 790.12	4859.76 $\pm$ 819.26
	<i>Inc-3</i>	8.81 $\pm$ 3.00	39.99 $\pm$ 6.31	209.70 $\pm$ 38.55	218.69 $\pm$ 25.83	1332.58 $\pm$ 316.15	3493.64 $\pm$ 62.70	4076.33 $\pm$ 671.42	5465.95 $\pm$ 1816.61
HOPSE-G	<i>Mix-1</i>	9.81 $\pm$ 2.93	54.94 $\pm$ 13.50	214.50 $\pm$ 7.54	198.45 $\pm$ 54.21	1288.78 $\pm$ 590.16	4201.85 $\pm$ 851.36	4315.76 $\pm$ 1097.48	6542.09 $\pm$ 1272.01
	<i>Mix-2</i>	7.63 $\pm$ 1.71	43.67 $\pm$ 18.29	229.05 $\pm$ 65.67	189.19 $\pm$ 45.39	1434.43 $\pm$ 547.60	3596.38 $\pm$ 519.37	3408.67 $\pm$ 162.45	5377.27 $\pm$ 185.49
	<i>Adj-1</i>	<b>4.56 <math>\pm</math> 0.62</b>	<b>25.49 <math>\pm</math> 6.16</b>	<b>92.97 <math>\pm</math> 27.48</b>	104.94 $\pm$ 28.21	542.03 $\pm$ 94.68	<b>1891.07 <math>\pm</math> 17.81</b>	<b>1885.35 <math>\pm</math> 28.06</b>	<b>2194.20 <math>\pm</math> 42.70</b>
	<i>Adj-2</i>	4.92 $\pm$ 0.37	32.03 $\pm$ 9.91	118.32 $\pm$ 17.84	111.18 $\pm$ 18.27	480.02 $\pm$ 100.70	2172.54 $\pm$ 216.62	2096.15 $\pm$ 33.94	2323.75 $\pm$ 222.16
	<i>Adj-3</i>	5.58 $\pm$ 1.28	39.85 $\pm$ 17.90	120.88 $\pm$ 31.47	134.65 $\pm$ 49.81	<b>478.06 <math>\pm</math> 107.13</b>	2302.00 $\pm$ 47.08	2385.63 $\pm$ 176.04	2997.61 $\pm$ 824.53
	<i>Inc-1</i>	5.80 $\pm$ 0.27	32.71 $\pm$ 8.43	130.06 $\pm$ 22.37	<b>106.98 <math>\pm</math> 27.98</b>	649.05 $\pm$ 114.28	2580.45 $\pm$ 47.63	2471.89 $\pm$ 47.46	3716.82 $\pm$ 1192.83
HOPSE-G	<i>Inc-2</i>	6.44 $\pm$ 0.54	32.98 $\pm$ 8.25	128.01 $\pm$ 22.39	<b>99.39 <math>\pm</math> 33.07</b>	661.57 $\pm$ 133.52	2489.63 $\pm$ 444.47	2240.50 $\pm$ 43.84	2568.75 $\pm$ 76.80
	<i>Inc-3</i>	6.85 $\pm$ 0.98	51.18 $\pm$ 11.23	174.20 $\pm$ 57.02	148.67 $\pm$ 37.09	778.78 $\pm$ 117.23	3038.25 $\pm$ 65.40	2930.43 $\pm$ 430.59	3602.56 $\pm$ 555.32
	<i>Mix-1</i>	6.85 $\pm$ 0.72	51.94 $\pm$ 9.59	209.07 $\pm$ 28.40	150.07 $\pm$ 36.64	911.69 $\pm$ 165.22	3408.18 $\pm$ 515.16	3379.79 $\pm$ 111.99	4321.64 $\pm$ 1094.92
	<i>Mix-2</i>	5.16 $\pm$ 0.36	35.97 $\pm$ 4.38	168.30 $\pm$ 38.75	142.36 $\pm$ 34.54	716.46 $\pm$ 53.19	3324.16 $\pm$ 1113.48	2794.73 $\pm$ 345.73	3876.34 $\pm$ 1141.15

## F.6 Runtime vs accuracy

Figure 5 provides a comparative overview of model performance in terms of F1 score against total training runtime for four benchmark tasks:  $\beta_1$  (a),  $\beta_2$  (b), NAME (c), and ORIENT (d). Figure 6 shows the same arrangement but from the perspective of average runtime per epoch against performance. Additionally, Figure 6 shows the convergence speed of any particular model. These results clearly show that HOPSE is the best model for an optimal trade-off between runtime and accuracy.

Table 11: Total runtime per neighborhood on *cell*. Results are shown as mean  $\pm$  standard deviation. The best result per domain and model is in **bold** and results within one standard deviation of the lowest per domain are highlighted in blue. On HOPSE-G, some more complex neighborhoods will result in faster time, even though they contain more information and thus parameters to be learned. This is one of the effects of convergence speed. This can be seen in neighborhoods *Mix-1* and *Mix-2*. On HOPSE-M, there is no such drastic difference

		Graph Tasks				
		MUTAG	PROTEINS	NCI1	NCI109	ZINC
Nbhd						
HOPSE-M	<i>Adj-1</i>	7.03 $\pm$ 0.86	37.52 $\pm$ 2.06	<b>144.11 <math>\pm</math> 32.07</b>	142.87 $\pm$ 45.01	1128.14 $\pm$ 166.57
	<i>Adj-2</i>	7.66 $\pm$ 0.82	<b>35.68 <math>\pm</math> 7.88</b>	147.04 $\pm$ 24.07	<b>121.89 <math>\pm</math> 18.30</b>	<b>901.44 <math>\pm</math> 203.17</b>
	<i>Adj-3</i>	9.78 $\pm$ 2.94	37.85 $\pm$ 10.19	153.94 $\pm$ 29.39	131.39 $\pm$ 36.31	1414.14 $\pm$ 325.91
	<i>Inc-1</i>	7.86 $\pm$ 0.54	37.06 $\pm$ 7.05	174.19 $\pm$ 33.02	190.50 $\pm$ 35.45	1173.43 $\pm$ 198.41
	<i>Inc-2</i>	<b>6.41 <math>\pm</math> 1.43</b>	36.82 $\pm$ 11.82	220.47 $\pm$ 55.22	128.32 $\pm$ 14.86	1020.04 $\pm$ 131.15
	<i>Inc-3</i>	8.30 $\pm$ 0.78	48.24 $\pm$ 18.26	169.79 $\pm$ 41.60	169.78 $\pm$ 37.03	1183.44 $\pm$ 217.72
HOPSE-G	<i>Mix-1</i>	8.83 $\pm$ 1.18	51.25 $\pm$ 13.72	205.54 $\pm$ 25.51	210.50 $\pm$ 11.62	1313.43 $\pm$ 132.16
	<i>Mix-2</i>	7.42 $\pm$ 1.37	44.34 $\pm$ 13.40	203.46 $\pm$ 48.75	193.17 $\pm$ 44.83	1676.92 $\pm$ 398.90
	<i>Adj-1</i>	5.09 $\pm$ 0.93	26.71 $\pm$ 4.79	<b>88.31 <math>\pm</math> 11.27</b>	95.95 $\pm$ 28.16	683.86 $\pm$ 125.70
	<i>Adj-2</i>	<b>4.98 <math>\pm</math> 0.47</b>	31.85 $\pm$ 5.43	96.33 $\pm$ 19.91	<b>93.98 <math>\pm</math> 15.00</b>	887.83 $\pm$ 160.74
	<i>Adj-3</i>	6.64 $\pm$ 0.89	31.13 $\pm$ 5.56	100.65 $\pm$ 14.14	113.39 $\pm$ 18.75	<b>595.39 <math>\pm</math> 107.46</b>
	<i>Inc-1</i>	5.75 $\pm$ 1.45	34.11 $\pm$ 7.89	110.19 $\pm$ 19.33	105.67 $\pm$ 27.00	767.42 $\pm$ 85.39
	<i>Inc-2</i>	7.65 $\pm$ 2.32	<b>24.65 <math>\pm</math> 6.74</b>	105.02 $\pm$ 28.61	126.14 $\pm$ 37.05	721.57 $\pm$ 60.10
	<i>Inc-3</i>	7.87 $\pm$ 1.47	44.42 $\pm$ 9.81	181.18 $\pm$ 96.45	<b>100.22 <math>\pm</math> 11.50</b>	896.86 $\pm$ 162.01
	<i>Mix-1</i>	7.61 $\pm$ 0.68	46.14 $\pm$ 10.02	239.59 $\pm$ 38.24	168.35 $\pm$ 50.01	671.40 $\pm$ 948.29
	<i>Mix-2</i>	5.27 $\pm$ 0.57	36.29 $\pm$ 13.05	152.73 $\pm$ 8.26	104.12 $\pm$ 37.76	1229.56 $\pm$ 527.27

## G Licenses

This work does not distribute existing datasets. However, the dataset it uses will be mentioned here along with their licenses. The *Graph* datasets MUTAG, PROTEINS, NCI1, NCI109 do not specify a license and are distributed as part of 'TUDatasets' accessed via <https://pubs.acs.org/doi/full/10.1021/acs.jcim.5b00559>. The ZINC dataset from <https://pubs.acs.org/doi/full/10.1021/acs.jcim.5b00559> is freely available. The MANTRA benchmarking dataset is licensed under the 3-Clause BSD license. The CSL dataset does not specify a particular license aside from the CC BY 4.0 from [17].

## H Author contributions.

M.C. led the implementation, developed the theoretical framework, performed data analysis, and drafted the manuscript. M.M. primarily contributed to the theoretical framework and manuscript writing. N.M. provided infrastructure and project support, and contributed to writing. L.T. and G.B. conceived the research idea, designed the study, analyzed the results, and contributed to manuscript preparation. Additionally, L.T. participated in the implementation and theoretical development, conducted experiments with M.C., and supervised the project.

Table 12: Preprocessing time per neighborhood on *simplicial*. Results are shown as mean time in seconds. The best result per domain and model is in **bold**. All *Topological Tasks* have the same time as they share the same preprocessing time. Times increase with neighborhood since with *Adj-1* being the fastest as it's the neighborhood of the underlying graph.

		Graph Tasks				Topological Tasks				
		Nbhd	MUTAG	PROTEINS	NCI1	NCI109	ZINC	NAME	ORIENT	$(\beta_0, \beta_1, \beta_2)$
HOPSE-M	<i>Adj-1</i>		<b>2.42</b>	<b>35.15</b>	<b>53.37</b>	<b>53.82</b>	<b>142.01</b>	<b>333.65</b>	<b>333.65</b>	<b>333.65</b>
	<i>Adj-2</i>		3.24	49.49	72.94	72.80	195.71	823.68	823.68	823.68
	<i>Adj-3</i>		3.26	58.49	74.16	73.40	199.37	973.49	973.49	973.49
	<i>Inc-1</i>		3.62	79.37	92.40	92.20	229.92	1121.78	1121.78	1121.78
	<i>Inc-2</i>		4.39	80.91	111.65	111.49	280.18	1544.42	1544.42	1544.42
	<i>Inc-3</i>		5.58	123.97	147.31	148.10	367.95	2233.27	2233.27	2233.27
	<i>Mix-1</i>		7.27	165.71	191.94	193.45	489.55	3724.43	3724.43	3724.43
	<i>Mix-2</i>		4.99	95.34	118.46	117.35	318.12	2495.14	2495.14	2495.14
	<i>Adj-1</i>		<b>4.54</b>	<b>45.94</b>	<b>103.91</b>	<b>103.47</b>	<b>297.61</b>	<b>913.38</b>	<b>913.38</b>	<b>913.38</b>
HOPSE-G	<i>Adj-2</i>		7.81	65.54	172.20	172.97	496.73	1676.79	1676.79	1676.79
	<i>Adj-3</i>		7.76	92.15	174.23	174.49	502.85	2742.26	2742.26	2742.26
	<i>Inc-1</i>		8.05	93.32	181.82	183.44	532.93	2654.36	2654.36	2654.36
	<i>Inc-2</i>		11.21	90.87	245.87	248.52	714.05	2813.64	2813.64	2813.64
	<i>Inc-3</i>		14.53	142.22	324.62	326.91	952.95	4432.76	4432.76	4432.76
	<i>Mix-1</i>		21.02	210.41	474.58	472.70	1381.15	7329.51	7329.51	7329.51
	<i>Mix-2</i>		14.28	160.55	314.86	319.78	932.91	5241.30	5241.30	5241.30

Table 13: Preprocessing time per neighborhood on *cell*. Results are shown as mean time in seconds. The best result per domain and model is in **bold**. Similarly to the case of *simplicial*, the fastest neighborhoods to precompute are the smallest ones.

		Graph Tasks					
		Nbhd	MUTAG	PROTEINS	NCI1	NCI109	ZINC
HOPSE-M	<i>Adj-1</i>		<b>2.81</b>	<b>27.16</b>	<b>59.68</b>	<b>60.07</b>	<b>163.66</b>
	<i>Adj-2</i>		3.75	40.70	81.96	82.60	221.18
	<i>Adj-3</i>		4.44	50.97	96.94	97.38	267.01
	<i>Inc-1</i>		4.97	74.99	120.83	121.33	310.83
	<i>Inc-2</i>		4.98	75.22	121.62	122.38	312.12
	<i>Inc-3</i>		7.07	116.00	182.49	179.43	461.41
	<i>Mix-1</i>		9.66	162.30	242.08	244.40	627.80
	<i>Mix-2</i>		7.04	89.45	159.44	160.62	441.84
	<i>Adj-1</i>		<b>5.08</b>	<b>38.04</b>	<b>113.21</b>	<b>108.81</b>	<b>315.07</b>
HOPSE-G	<i>Adj-2</i>		8.34	58.50	189.71	184.54	525.01
	<i>Adj-3</i>		11.10	75.56	253.63	248.51	727.66
	<i>Inc-1</i>		11.89	85.26	264.02	259.75	734.69
	<i>Inc-2</i>		11.81	120.32	292.64	257.43	740.39
	<i>Inc-3</i>		18.51	132.25	420.45	403.67	1163.78
	<i>Mix-1</i>		28.02	188.99	641.07	621.33	1776.32
	<i>Mix-2</i>		20.47	140.60	472.04	460.79	1326.40

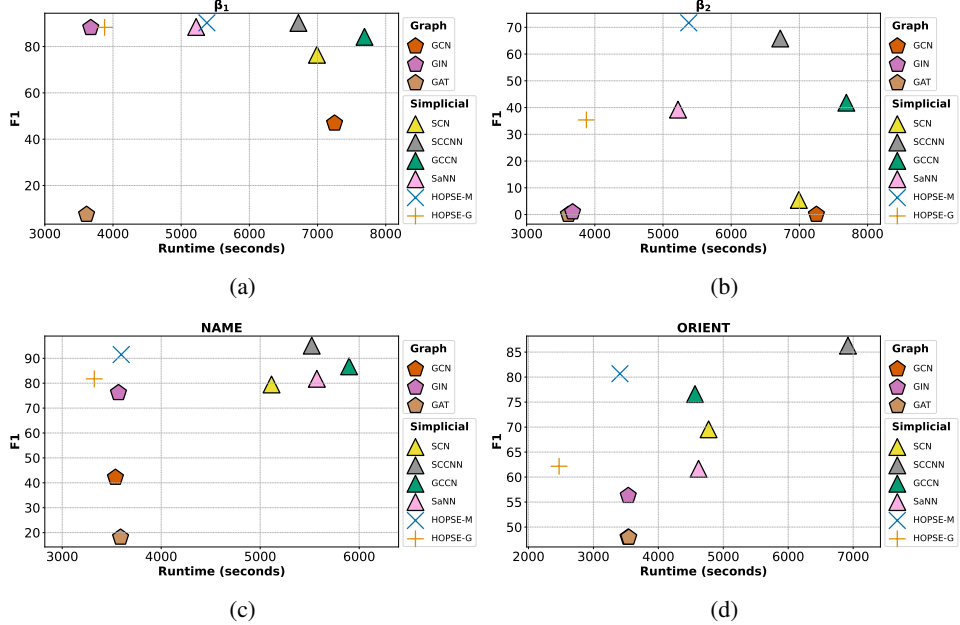


Figure 5: Total runtime vs F1 accuracy on the MANTRA benchmarks. **HOPSE-G** (+) is consistently faster than GNNs while generally outperforming them, being a reliable choice for efficiency/performance trade-off. **HOPSE-M** (x) generally outperforms all models (even GNNs in some cases) while being significantly faster than the *simplicial* alternatives in terms of performance for a slight performance trade-off.

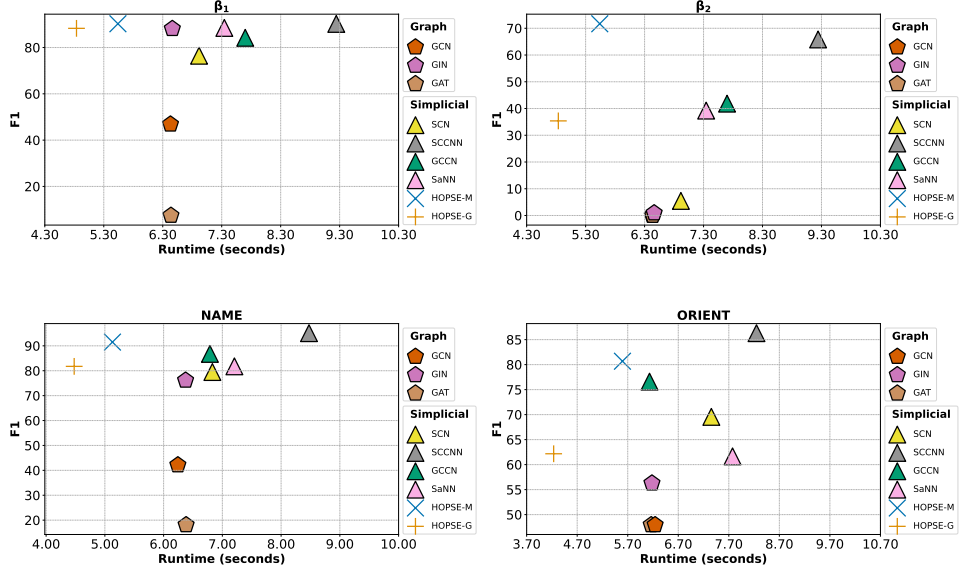


Figure 6: Validation runtime vs F1 accuracy on the MANTRA benchmarks. Across all cases, **HOPSE-G** (x) consistently occupies the upper-left region of the plots, indicating superior performance with relatively lower runtime. This trend is particularly evident for the  $\beta_1$ , NAME, and ORIENT datasets, where **HOPSE-M** achieves the highest F1 scores while requiring substantially less training time compared to other simplicial baselines like GCCN and SCCNN. Interestingly, GIN performs really well on  $\beta_1$  and even though it's per-epoch slower than **HOPSE-G** and **HOPSE-M** (x), it converges faster, resulting in a slightly lower run-time.